AGU PUBLICATIONS

JGR

Journal of Geophysical Research: Space Physics

RESEARCH ARTICLE
10.1002/2016JA023790

Key Points:
- Intercomparison of three X line models' performances on predicting the direction of reconnection jets observed at the dayside magnetopause
- The X line model based on maximization of the asymmetric reconnection outflow speed fits a slightly higher percentage of the observed jets
- Several Earth radii long X lines are shown to organize reconnection jet observations at locations far apart

Correspondence to:
V. M. Souza,
vitor.souza@inpe.br

Citation:
Souza, V. M., W. D. Gonzalez, D. G. Sibeck, D. Koga, B. M. Walsh, and O. Mendes (2017), Comparative study of three reconnection X line models at the Earth's dayside magnetopause using in situ observations, *J. Geophys. Res. Space Physics*, *122*, 4228–4250, doi:10.1002/2016JA023790.

Received 8 DEC 2016
Accepted 22 MAR 2017
Accepted article online 27 MAR 2017
Published online 12 APR 2017

Comparative study of three reconnection X line models at the Earth's dayside magnetopause using in situ observations

V. M. Souza[1], W. D. Gonzalez[1], D. G. Sibeck[2], D. Koga[1], B. M. Walsh[3], and O. Mendes[1]

[1]National Institute for Space Research, São José dos Campos, Brazil, [2]NASA/Goddard Space Flight Center, Greenbelt, Maryland, USA, [3]Department of Mechanical Engineering and Center for Space Physics, Boston University, Boston, Massachusetts, USA

Abstract This work examines the large-scale aspects of magnetic field reconnection at the Earth's dayside magnetopause. We use two sets of reconnection events, which are identified mostly by the in situ detection of accelerated and Alfvénic plasma flows. We intercompare three analytical models that predict the reconnection X line location and orientation, namely, the Trattner et al. (2007) and Swisdak and Drake (2007) models and also a modified version of the component merging model. In the first set of reconnection observations, we show three fortuitous, quasi-simultaneous dayside magnetopause crossing events where two widely separated spacecraft detect reconnection signatures, and the X line location and orientation can be inferred from the observations. We compare X line model predictions to those inferred from observations. These three reconnection events indicate the presence of an extended (>7 Earth radii in length), component-type reconnection X line on Earth's dayside magnetopause connecting and structuring the reconnection signatures at locations far apart. In the second set of reconnection events, we analyze the X line models' performance in predicting the observed reconnection outflow direction, i.e., its north-south and/or east-west senses, in a total of 75 single, rather than multiple and quasi-simultaneous, magnetopause crossing events, where reconnection-associated plasma flows were clearly present. We found that the Swisdak and Drake's (2007) X line model performs slightly better, albeit not statistically significant, when predicting both accelerated plasma flow north-south and east-west components in 73% and 53% of the cases, respectively, as compared to the Trattner et al. (2007) model (70% north-south and 42% east-west) and the modified component merging model (66% north-south and 50% east-west).

1. Introduction

Magnetic reconnection between the magnetosheath and Earth's magnetic fields is the primary mechanism by which momentum, mass, and energy are transferred from the solar wind into the magnetosphere. Reconnection occurs along the dayside magnetopause—a boundary that separates the cold (~100 eV) and dense (~20 cm^{-3}) magnetosheath plasma from the hot (~10 keV) and tenuous (~0.2 cm^{-3}) magnetosphere plasma [e.g., *Sibeck et al.*, 1999].

A large body of evidence [cf. *Paschmann et al.*, 2013, and references therein] points to a scenario where reconnection operates at the dayside magnetopause along extended (many Earth radii—R_E—long) and long-lasting (from tens of minutes up to few hours) X lines wherein the topologies of the interacting magnetic fields are changed during the magnetic reconnection process. Quasi-simultaneous multipoint observations of reconnection signatures at distinct local times, in particular the directions of accelerated plasma flows (also known as *jets*), are important to address whether reconnection operates on different regions of the Earth's dayside magnetopause and therefore can be used to provide some information regarding the large-scale aspects of reconnection. There are only a few cases, though, reported in the literature where such multi-spacecraft conjunctions were found, mostly because the chances for finding them are exceedingly small due to highly variable interplanetary magnetic field (IMF) conditions, as pointed out by *Phan et al.* [2006].

Observational evidence for an extended reconnection X line has been provided by *Phan et al.* [2006] in the form of mainly northward reconnection jets detected quasi-simultaneously by two widely separated spacecraft. The observed jet directions at the two spacecraft locations were in agreement with the presence

of a tilted and subsolar X line located somewhere southward of both spacecraft locations, as predicted by standard component reconnection models [*Sonnerup*, 1974; *Gonzalez and Mozer*, 1974]. *Dunlop et al.* [2011] reported an event where the Time History of Events and Macroscale Interactions during Substorms (THEMIS) A and Double Star TC-1 spacecraft have crossed the dayside magnetopause duskward and dawnward of the noon-midnight meridian plane, respectively, within 2 min from each other. The reconnection signatures detected at the two far apart spacecraft were consistent with an extended (~9 R_E long), tilted, and subsolar X line which was very close to the TC-1 location and southward from the THEMIS A location. Yet another fortuitous instance of large-scale dayside magnetopause reconnection taking place under substantially asymmetric magnetospheric plasma conditions was provided by *Walsh et al.* [2014] via a near-simultaneous conjunction of two THEMIS spacecraft separated by 1.5 h in magnetic local time (MLT). The observed plasma jets were consistent with both spacecraft being near the assumed subsolar X line since both positive and negative enhancements in the major tangential (to the magnetopause) north-south component of the flow were detected. Such flows, which are known by jet reversals, give important indications about the position of the reconnection X line [*Trenchi et al.*, 2008; *Trattner et al.*, 2012].

As exemplified above, unidirectional reconnection jets, as opposed to jet reversals, give information only on the expected X line location relative to the spacecraft location, but it cannot precisely determine where the X line (or reconnection region) really is located. Some attempts to remotely locate the reconnection region have been done [e.g., *Trattner et al.*, 2007, 2012] using additional information like 2-D cuts through 3-D velocity distribution functions. In an effort to establish where reconnection should occur, both analytical and numerical models have been proposed [see, e.g., *Sonnerup*, 1974; *Gonzalez and Mozer*, 1974; *Moore et al.*, 2002; *Trattner et al.*, 2007; *Swisdak and Drake*, 2007; *Laitinen et al.*, 2007; *Komar et al.*, 2013]. Each predicts the X line location and orientation along current sheets which separate distinct magnetized plasmas, with the Earth's dayside magnetopause being the most common example.

Each X line model chooses a single or a set of parameters which should govern the X line location and orientation. Earlier models, like the component merging model proposed by *Gonzalez and Mozer* [1974] and *Sonnerup* [1974], advocate that the X line location should coincide with that of a subsolar streamline of the magnetopause Chapman-Ferraro current density. For negative values of the IMF north-south (B_z) component, such an X line would always cross the subsolar point, extending from the northern (southern) dusk hemisphere to the southern (northern) dawn hemisphere whenever the east-west IMF B_y component is positive (negative) [*Sibeck and Lin*, 2011]. If the IMF has a purely southward orientation, the dayside X line location should extend throughout the dayside region and coincide with the magnetic equator whenever the Earth's magnetic dipole axis is perpendicular to the Earth-Sun line. When this condition is not met, however, the X line passes only through the subsolar point and has a tilt relative to the magnetic equator [*Gonzalez and Mozer*, 1974; *Sonnerup*, 1974]. The *Trattner et al.* [2007] model, on the other hand, proposes that the X line should follow the loci along the Earth's dayside magnetopause where the magnetic shear angle between the adjacent (to the magnetopause) magnetosheath and magnetospheric magnetic fields maximizes. For IMF $B_y \neq 0$ conditions, the *Trattner et al.* [2007] X line location prediction near the subsolar region would be somewhat similar to that of *Gonzalez and Mozer* [1974] and *Sonnerup* [1974] only in the sense that the X line location should respond to nonzero IMF B_y conditions by making a tilt relative to the y_{GSM} axis. In the *Swisdak and Drake*'s [2007] model maximizing the asymmetric reconnection outflow speed is the controlling factor for the location and orientation of the X line. In their model, the outflow speed is derived on the basis of two-dimensional, time-stationary MHD theory, and it is found to be a function of both upstream magnetic field and densities. All these X line model location predictions can then be directly compared with the X line locations inferred from reconnection jet observations and/or other reconnection signatures. It is worthwhile to mention that in contrast to all the X line models examined in this paper that predict that the position of the X line is steady when the plasma/magnetic field conditions in the magnetosheath are stable, the diamagnetic drift can be responsible for a motion of the X line also during stable magnetosheath conditions, when the IMF B_y component is large [*Swisdak et al.*, 2003, 2010; *Trenchi et al.*, 2015].

Some previous studies have been conducted trying to validate X line models against in situ reconnection observations. *Trenchi et al.* [2008] showed reconnection jet directions from 149 Double Star TC-1's magnetopause crossings consistent with subsolar X lines tilted according to the observed magnetosheath clock angle, which in turn agrees with the component reconnection hypothesis [*Sonnerup*, 1974; *Gonzalez and Mozer*, 1974]. Using a set of 15 magnetopause crossings from the Cluster mission with clear reconnection signatures, *Fuselier et al.* [2011] showed that the expected X line locations were in agreement with the

Trattner et al. [2007] maximum magnetic shear angle X line model in 13 cases. *Hoilijoki et al.* [2014] showed that the *Laitinen et al.*'s [2007] four-field line X line model location was in agreement with the expected X line location inferred from THEMIS A and Double Star TC-1 observations reported by *Dunlop et al.* [2011]. To the best of our knowledge, however, there is no previous work in which an intercomparison of X line model performances against in situ reconnection jet observations was made. Previous statistical studies have been conducted analyzing the global pattern of reconnection jets at the Earth's dayside magnetopause and their dependence on the IMF orientation and magnetosheath's magnetic field and plasma parameters [*Scurry et al.*, 1994; *Pu et al.*, 2007]. We note that *Komar et al.* [2015] compared locations from six X line models against the magnetic separator [*Komar et al.*, 2013] location in global magnetospheric simulations. The magnetic separator corresponds to locations at the Earth's dayside magnetopause where four distinct magnetic field topologies meet, i.e., 1—"open" solar wind field lines whose foot points are not connected to the Earth but to the Sun; 2 and 3—half-open field lines with one end into the solar wind and the other end in either the Northern Hemisphere or Southern Hemisphere, and 4—closed field lines, whose both ends are attached to the Earth's ionosphere [*Komar et al.*, 2013]. We emphasize, however, that no in situ reconnection observations were used in the *Komar et al.* [2015] study.

Low-altitude observations can also be used to provide information regarding the spatial extent of the reconnection X line. In this regard, *Pinnock et al.* [2003] have sought such information in ground radar data. By using a conjunction of Super Dual Auroral Radar Network (SuperDARN) and Defense Meteorological Satellite Program (DMSP) F13 plasma drift velocities data during a 30 min period with a steady southward IMF B_z component, *Pinnock et al.* [2003] reported ionospheric signatures of dayside magnetopause reconnection spanning 10 h of MLT over the whole analyzed interval. The implied X line extent was found to be ~38 R_E which was in close agreement with the expected X line's length (40 R_E) determined by *Phan et al.* [2000, 2001] for the same reconnection event.

This work is divided into two parts. In the first, the macroscale aspect of magnetic reconnection at Earth's dayside magnetopause is addressed by analyzing three fortuitous, quasi-simultaneous magnetopause crossing events where two widely separated spacecraft detected accelerated and Alfvénic plasma flows on the earthward side of the magnetopause. We make use of well-known models which predict both the X line location and orientation, namely, those of *Trattner et al.* [2007] and *Swisdak and Drake* [2007], as well as a modified version of the component merging model [*Gonzalez and Mozer*, 1974; *Sonnerup*, 1974]. The purpose is to verify, for each event, whether the two in situ observed jet's directions can be explained by a single, extended X line. The second part of this work is concerned with an intercomparison of the three X line model performances in predicting observed reconnection jet directions obtained during many magnetopause crossings of a single, rather than two, spacecraft. We gathered 75 of such crossings for a variety of IMF orientations using data from the THEMIS mission. We emphasize that any of the chosen X line models provide a prediction of the reconnection outflow *direction*. The jet direction predictions are based on the simple assumption that the reconnection outflow direction should be locally perpendicular to the local X line direction. In what follows, the instrumentation and methodology used are presented in section 2, the results of our analysis in section 3, and lastly, the summary and discussions are shown in section 4.

2. Instrumentation and Methodology

We have used data provided by eight spacecraft: Double Star TC-1 [*Liu et al.*, 2005], two of the Cluster mission [*Escoubet et al.*, 2001], i.e., Cluster 3 and 4, and five from the THEMIS mission [*Angelopoulos et al.*, 2008], THEMIS A, B, C, D, and E. Double Star TC-1 4 s resolution spin-averaged magnetic field data were obtained by the Fluxgate Magnetometer (FGM) instrument [*Carr et al.*, 2005], whereas the electron and ion plasma data were provided, respectively, by the Plasma Electron and Current Experiment instrument [*Fazakerley et al.*, 2005] and the Hot Ion Analyzer (HIA) instrument [*Réme et al.*, 2005]. Magnetic field data from Cluster 3 and 4 were provided at ~4 s spin resolution by the Fluxgate Magnetometer (FGM) instrument [*Balogh et al.*, 2001], whereas ion plasma data were obtained by both analyzers of the Cluster Ion Spectrometry (CIS) instrument [*Réme et al.*, 2001]: CIS-CODIF (Composition and Distribution Function analyzer) for Cluster 4, and CIS-HIA (Hot Ion Analyzer) for Cluster 3. For the THEMIS spacecraft, ~3 s spin resolution magnetic field data from the Fluxgate Magnetometer (FGM) instrument [*Auster et al.*, 2008] were used. For the plasma measurements on board the THEMIS both the Ion and Electron Electrostatic Analyzer (IESA and EESA) instruments [*McFadden et al.*, 2008] with ~3 s spin resolution were used. Magnetic field measurements on board the Active Composition Explorer

(ACE) spacecraft [*Stone et al.*, 1998] were also used, although they are not shown here. Next, the process to identify reconnection is presented.

2.1. Walén Test

The Walén relation establishes a way of testing whether the change in velocity undergone by the plasma constituents when crossing a discontinuity separating different magnetized plasma regimes is due to the effect of tangential (to the discontinuity) magnetic stresses expected in a rotational discontinuity [*Hudson*, 1970]. The derivation of the Walén relation consists in considering the discontinuity, i.e., the magnetopause, as a locally one-dimensional, time-stationary, and infinitesimally thin, ideal MHD layer known as rotational discontinuity.

$$\Delta\mathbf{V}_{\text{predicted}} = \mathbf{V}_2 - \mathbf{V}_1 = \pm\left(\frac{1-\alpha_1}{\mu_o\rho_1}\right)^{1/2}\left[\mathbf{B}_2\left(\frac{1-\alpha_2}{1-\alpha_1}\right) - \mathbf{B}_1\right]. \tag{1}$$

Equation (1) is known as the Walén relation, where the observed plasma flow change ($\Delta\mathbf{V}_{\text{observed}} = \mathbf{V}_2 - \mathbf{V}_1$) is compared against the predicted flow change ($\Delta\mathbf{V}_{\text{predicted}}$). The parameters μ_o, ρ, and $\alpha = (P_{\parallel} - P_{\perp})\mu_o/B^2$ are the magnetic permeability of free space, the plasma mass density, and the thermal pressure anisotropy factor, with $P_{\parallel}$ and $P_{\perp}$ being, respectively, the thermal pressures parallel and perpendicular to the local magnetic field vector **B**. Subscript 1 denotes the magnetosheath side of the magnetopause, whereas subscript 2 denotes the outflow jet region. If the spacecraft crosses the magnetopause above (below) the reconnection X line, the plus (minus) sign is taken in equation (1). The magnetosheath parameters (α_1, ρ_1, $\mathbf{B}_1$, and $\mathbf{V}_1$) are obtained as 1 min averages taken as close (in time) as possible to the magnetopause, and right after the magnetic field has completed its rotation through the magnetopause boundary, which in turn is identified when the reconnecting (B_L) component of the magnetic field changes sign. The observed jet velocity is obtained in the following way: first, we look for the instant t_{max} when the maximum plasma velocity magnitude, $\mathbf{V}_{\text{max}}$, is observed. Such an instant usually occurs when the spacecraft is on the earthward side of the dayside magnetopause boundary for asymmetric reconnection. Second, a 1 min average plasma velocity vector from the magnetosheath side of the magnetopause is taken using the same magnetosheath interval mentioned above. This averaged velocity vector is considered to be the background magnetosheath flow, $\mathbf{V}_{\text{background}}$. The observed jet velocity is considered to be given by

$$\Delta\mathbf{V}_{\text{observed}} = \mathbf{V}_{\text{max}} - \mathbf{V}_{\text{background}} \equiv \mathbf{V}_{\text{jet}}. \tag{2}$$

When subtracting the background velocity from the maximum observed velocity, we are assuming that the remaining term is due to the magnetic reconnection process alone. The remainder terms used to compose the predicted jet velocity $\Delta\mathbf{V}_{\text{predicted}}$, i.e., $\mathbf{B}_2$ and α_2, are taken at the instant t_{max} where the maximum plasma flow is observed.

We use the ΔV_A^* parameter which is a quality measure of the agreement between observed and predicted flow acceleration, and it is given by

$$\Delta V_A^* = \frac{\Delta\mathbf{V}_{\text{observed}} \cdot \Delta\mathbf{V}_{\text{predicted}}}{|\Delta\mathbf{V}_{\text{predicted}}|^2} = r_{\text{op}}\cos(\theta_{\text{op}}). \tag{3}$$

$\Delta V_A^* = 1$ means perfect agreement with theory, while lower ΔV_A^* values indicate a poorer agreement. The r_{op} and θ_{op} parameters refer to the observed to predicted flow ratio, $r_{\text{op}} = |\Delta\mathbf{V}_{\text{observed}}|/|\Delta\mathbf{V}_{\text{predicted}}|$, and the angular displacement of the observed jet direction from the predicted (magnetic field-aligned) direction, $\theta_{\text{op}} = \cos^{-1}[\Delta\mathbf{V}_{\text{observed}} \cdot \Delta\mathbf{V}_{\text{predicted}}/|\Delta\mathbf{V}_{\text{observed}}||\Delta\mathbf{V}_{\text{predicted}}|]$.

In order to positively identify reconnection to be occurring, we require the parameter ΔV_A^* to be larger than or equal to 0.5 as done in *Phan et al.* [2013]. If $\Delta V_A^* < 0.5$, further confirmation is required, and this will be discussed below when needed.

2.2. Reconnection X line Models

2.2.1. Maximum Magnetic Shear Angle: *Trattner et al.* [2007]

Following the property that magnetic reconnection has a higher chance to occur when the reconnecting magnetic fields are precisely oppositely directed, *Trattner et al.* [2007] proposed a theory whereby the location over the dayside magnetopause where reconnection should occur would be such that the local shear angle θ_{shear} between the reconnecting magnetic fields of the magnetosphere and magnetosheath regions is maximized. This idea has its foundations in the work of *Crooker* [1979] which was extended and tested by *Luhmann et al.* [1984] for a variety of IMF orientations using more realistic models of both magnetospheric

and magnetosheath magnetic fields. The *Trattner et al.* [2007] X line model is an improvement over the *Crooker* [1979] antiparallel reconnection model since it considers the subsolar magnetopause as a likely region for reconnection to occur when the IMF B_y component is nonzero [*Trattner et al.*, 2007]. The maximum shear angle model has been shown to correctly predict the X line location and orientation for some magnetic reconnection events observed by the THEMIS spacecraft [*Trattner et al.*, 2012].

To construct the maximum shear X line along an analytical and paraboloidal magnetopause, *Trattner et al.* [2007] employ the *Cooling et al.* [2001] and *Tsyganenko and Stern* [1996] models for generating the magnetosheath ($\mathbf{B}_{sh}$) and magnetospheric ($\mathbf{B}_{sp}$) magnetic fields, respectively. Here we use the self-consistent, 3-D global MHD Solar Wind Modeling Framework/Block-Adaptive-Tree Solar-wind Roe-type Upwind Scheme (BATS-R-US [*Tóth et al.*, 2011]) code to estimate the magnetic fields on both sides of the magnetopause boundary and then determine the magnetic shear angle θ_{shear}:

$$\theta_{shear} = \cos^{-1}\left[\frac{\mathbf{B}_{sp}\cdot\mathbf{B}_{sp}}{|\mathbf{B}_{sp}||\mathbf{B}_{sh}|}\right] \tag{4}$$

at each point of the modeled dayside magnetopause. A brief description of the MHD model used is presented in section 2.2.4.

2.2.2. Maximum Magnetopause Current Density: Modified Component Merging Model

Originally, *Gonzalez and Mozer* [1974] and *Sonnerup* [1974] proposed that the dayside reconnection X line would be best represented by a subsolar streamline of the Chapman-Ferraro current density, $\mathbf{J}_{CF}$, of the magnetopause. The subsolar Chapman-Ferraro current streamline would behave like a tilted line relative to the y_{GSM} axis for IMF orientations in which the B_y component is nonzero. Such an X line model has been shown to structure Double Star TC-1's reconnection jet observations for a variety of IMF orientations [see, e.g., *Trenchi et al.*, 2008].

Here we consider a modified version of the original component merging model of *Gonzalez and Mozer* [1974] and *Sonnerup* [1974] wherein the X line is a collection of points where the magnetopause current density magnitude, $|\mathbf{J}_{MP}|$, as modeled by the BATS-R-US code, is a maximum. There have been works [see, e.g., *Semenov and Pudovkin*, 1985; *Alexeev et al.*, 1998] which advocate the idea that dayside magnetopause reconnection would be initiated in places where the current density magnitude would surpass a certain threshold and, as a result, current-driven instabilities would provide an anomalous resistivity required for the reconnection process to proceed in a higher rate. With this choice, we remove the requirement that the X line must cross the subsolar point. The maximum magnetopause current density hypothesis for the X line location has been tested in global magnetospheric simulations [*Komar et al.*, 2015] against magnetic separator locations [*Komar et al.*, 2013]. Here we investigate the maximum magnetopause current density model performance against in situ reconnection jet observations. We use the current density vector modeled by the BATS-R-US code. At each point of the modeled magnetopause, the current density magnitude, J_{MP}, is calculated and stored.

2.2.3. Maximum Outflow Speed: *Swisdak and Drake* [2007]

In this model the X line should be located over the dayside magnetopause in such a way that at each point, the reconnection outflow speed, V_{out}, which is a function of the local magnetic fields and plasma densities on both sides of the magnetopause boundary, maximizes. The reconnection outflow speed is derived from 2-D time-stationary MHD theory and is given by [*Swisdak and Drake*, 2007]

$$V_{out} = \sqrt{\frac{B_{sp}\sin\alpha_{SD} + B_{sh}\sin(\theta_{shear}-\alpha_{SD})}{\mu_o\left(\frac{\rho_{sh}}{B_{sh}\sin\alpha_{SD}} + \frac{\rho_{sp}}{B_{sp}\sin(\theta_{shear}-\alpha_{SD})}\right)}}, \tag{5}$$

where α_{SD} is the angle between the X line and the local model geomagnetic field vector $\mathbf{B}_{sp}$. Thus, each point pertaining to this X line model satisfies the extremum condition $\partial V_{out}/\partial\alpha_{SD}=0$, where $0\le\alpha_{SD}\le\theta_{shear}$. A generic configuration of both magnetic field orientations and the angles presented in equation (5) is shown in Figure 1. The magnetospheric and magnetosheath magnetic fields are evaluated at the local reconnection plane, represented here by the $L-M$ plane in the boundary normal coordinates which is tangential to the local magnetopause surface. Our method for determining the magnetopause location in the BATS-R-US model, the densities, and magnetic field vectors on both sides of the modeled magnetopause boundary, and how we determine V_{out}, are shown in the following section.

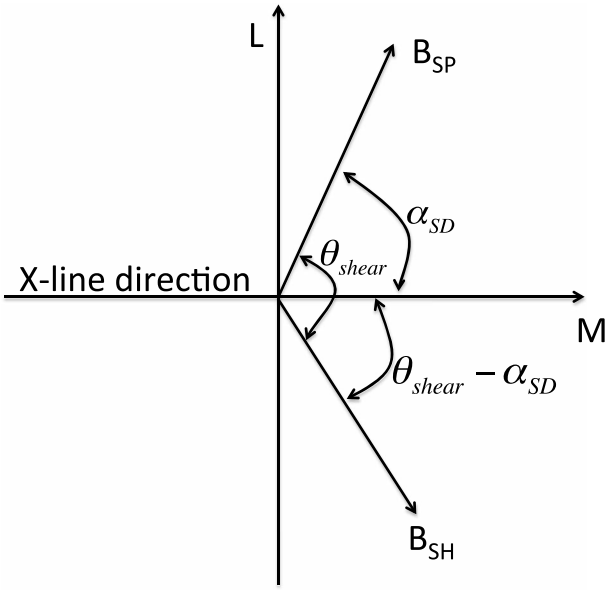

Figure 1. Generic magnetosphere ($\mathbf{B}_{sp}$) and magnetosheath ($\mathbf{B}_{sh}$) magnetic fields configuration in the reconnection (*LM*) plane on the dayside magnetopause and the angles they make between them and with the X line (*M*) direction as obtained by the *Swisdak and Drake* [2007] X line model.

2.2.4. Global MHD Runs and Algorithm for X Line Location Determination

As mentioned in the previous sections, the parameters required for determining the X line location prediction in each of the three models used here were obtained by means of the BATS-R-US code [*Tóth et al.*, 2011, and references therein]. The set of ideal MHD equations is solved on a three-dimensional, adaptive Cartesian grid in which the cell size increases away from the Earth in factors of 2. The highest grid resolution employed was 0.25 R_E in the domain $-15 \le \xi \le 15$ R_E, where $\xi = x$, y, and z GSM coordinates. We ran the code for 2 h using static input solar wind conditions and a static tilt of the Earth's dipole field. Only the final output files, i.e., those on the 02:00 hour mark, were used for further analysis. For the first set of three quasi-simultaneous reconnection events, the respective IMF and dipole tilt conditions used as input for BATS-R-US are shown in Table 1. As for the second set of reconnection events, the input IMF and dipole tilt conditions will be discussed in section 3.2.2. The BATS-R-US code was run by using the computational resources from the Coordinated Community Modeling Center (CCMC, http://ccmc.gsfc.nasa.gov/index.php) at NASA/Goddard Space Flight Center. We note that for all BATS-R-US runs used in this work we have used static solar wind density ($n = 5$ cm^{-3}), velocity ($\mathbf{V} = -400\hat{\mathbf{x}}$ km/s), and temperature ($T = 2 \times 10^5$ K) conditions.

Next, we describe how we determine V_{out} and the magnetic field and plasma parameters involved in its calculation. A particular BATS-R-US magnetopause location is determined by taking the first current density maximum along a given radial profile. This process is repeated for the whole dayside region, i.e., $-90° \le \phi \le 90°$ and $0° \le \theta \le 180°$, which is discretized on equally spaced steps ($\Delta\phi = \Delta\theta = 1.8°$), where ϕ and θ are, respectively, the azimuthal and polar angles of standard spherical coordinates. At a given magnetopause location, we take the magnetic field and density parameters on both sides of the magnetopause boundary along the local normal vector, which for simplicity is considered to be represented by the local radial vector (see *Souza* [2015] for details). Magnetospheric (magnetosheath) parameters are taken at a 1 R_E distance inside (outside) the magnetopause boundary along the radial direction. Such a large distance ensures that we are correctly sampling the sought after parameters in their respective regions, as presented in Figure 2 which shows (top) equatorial and (bottom) meridional cuts of the magnetospheric environment, as modeled by the BATS-R-US

Table 1. Three Quasi-Simultaneous Magnetopause Crossing Events and Some Key Parameters Such as Location of Each Spacecraft When the Magnetopause Was Crossed; Earth's Dipole Tilt (ψ) Inclination as Obtained by the Geopack (http://ampere.jhuapl.edu/code/idl_ geopack.html) Package; Interplanetary Medium Conditions, i.e., IMF Components and Dynamic Pressure P_{dyn}; the Plasma Jet Magnitude V_{jet}; the Observed to Predicted Jet Magnitude Ratio r_{op}; the Angular Displacement of the Observed Jet Direction From the Field-aligned Direction θ_{op}; and the ΔV_A^* Parameter

S/C	Position (R_E)			Magnetopause Crossing Time	Tilt (ψ)	IMF (nT)			P_{dyn} (nPa)	V_{jet} (km/s)	r_{op}	θ_{op}	$\Delta V_A^* = r_{op} \cos\theta_{op}$
	X_{GSM}	Y_{GSM}	Z_{GSM}			B_x	B_y	B_z					
Cluster 4	8.5	1.3	4.5	2007-3-5/19:14:00	2.7°	−4.02	1.26	−4.48	2.05	321	0.60	24.05°	0.55
Double Star	5.8	9.1	3.2	2007-3-5/19:05:00	✓	✓	✓	✓	✓	322	0.77	22.4°	0.71
Cluster 3	6.9	−8.6	−3.1	2009-5-22/16:22:00	30.5°	−4.34	1.99	−2.75	1.71	206	0.54	26.62°	0.49
THEMIS B	7.3	8.8	−0.4	2009-5-22/16:26:00	✓	✓	✓	✓	✓	240	0.64	2.76°	0.64
THEMIS A	4.0	10.8	−4.0	2009-7-7/14:45:00	30.7°	−2.11	3.79	−2.87	2.22	198	0.90	13.57°	0.87
THEMIS C	9.1	2.8	−3.1	2009-7-7/14:39:00	✓	✓	✓	✓	✓	244	0.70	0.48°	0.70

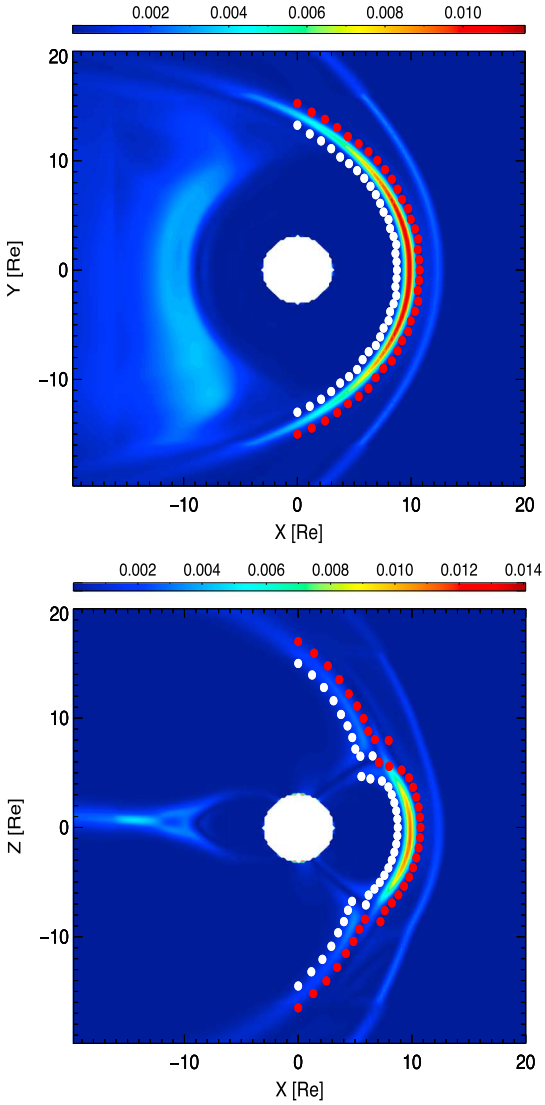

Figure 2. Color contour plots of the BATS-R-US current density magnitude in units of $\mu A/m^2$ in the (top) equatorial ($Z = 0$) plane and (bottom) the noon-meridian ($Y = 0$) plane. White (red) circles refer to locations at 1 R_E distance, along the local normal vector, earthward (sunward) of the BATS-R-US magnetopause boundary where the magnetospheric (magnetosheath) parameters are sampled for further analysis. The local normal vector is approximated here by the local radial vector. Even with this approximation, the sought parameters are taken well inside the region where they are supposed to be sampled.

code. After this step the only remaining quantity to be found is the angle α_{SD}. Once B_{sp}, B_{sh}, ρ_{sp}, and ρ_{sh} are found for a given magnetopause location, they are substituted in equation (5), so we end up with V_{out} as a function of α_{SD} only. We then cause α_{SD} to vary between 0° and θ_{shear} in order to find the α_{SD} that maximizes V_{out}. This process is repeated for all dayside magnetopause locations, always storing the correspondent V_{out} value. One can visualize the final result as a map of V_{out} values over the BATS-R-US dayside magnetopause boundary projected into the $x_{GSM} = 0$ plane, as presented in Figure 3c. Similar maps are obtained for the magnetopause current density magnitude J_{MP} (Figure 3a) and the magnetic shear angle θ_{shear} (Figure 3b).

The next step is to find the X line location for each of the three X line models used in this work. Like *Komar et al.* [2015], we employ an image processing technique [*Lindeberg*, 1993, 1998]. The purpose of the algorithm is to find the ridge of local maxima of a 2-D image $\eta(y, z)$, where η can be any of the three parameters θ_{shear}, J_{MP}, or V_{out}. Such an image is obtained when we project the analyzed parameter into the $x_{GSM} = 0$ plane, as shown in Figure 3. In the case depicted in Figure 3, the static IMF and Earth's dipole tilt conditions used were, respectively, $(B_x, B_y, B_z) = (5.0, 5.0, -2.886)$ nT and $\psi = 0°$. One can see that the X line location (black circles) determined by the ridge-detection algorithm in this case, and, in fact, at all other cases, is in agreement with the characteristics of a component-type reconnection X line [*Gonzalez and Mozer*, 1974; *Sonnerup*, 1974]. That means for positive IMF B_y and negative IMF B_z components, the X line tilt relative to the equator must be such that the X line should extend from the northern dusk into the southern dawn sectors of the magnetosphere, as it is the case of the X lines shown in Figure 3.

3. Results

3.1. First Set of Reconnection Events: Quasi-Simultaneous Magnetopause Crossings

We have found three fortuitous events where two widely separated spacecraft crossed the dayside magnetopause quasi-simultaneously. For these events, ground radar data coverage in MLT sectors other than those covered by the two satellites was not available, which would have enabled an analysis like that done by *Pinnock et al.* [2003].

Table 1 summarizes the main characteristics of the three reconnection events reported here, such as magnetopause crossing times, spacecraft locations at the magnetopause, prevailing solar wind conditions, and the parameters for the Walén relationship calculation. Solar wind conditions were determined by using 1 min time resolution data from the OMNI database [*King and Papitashvili*, 2005]. In particular, the values shown in Table 1 for the IMF and dynamic pressure were obtained as 20 min averages taken prior to one of the spacecraft in

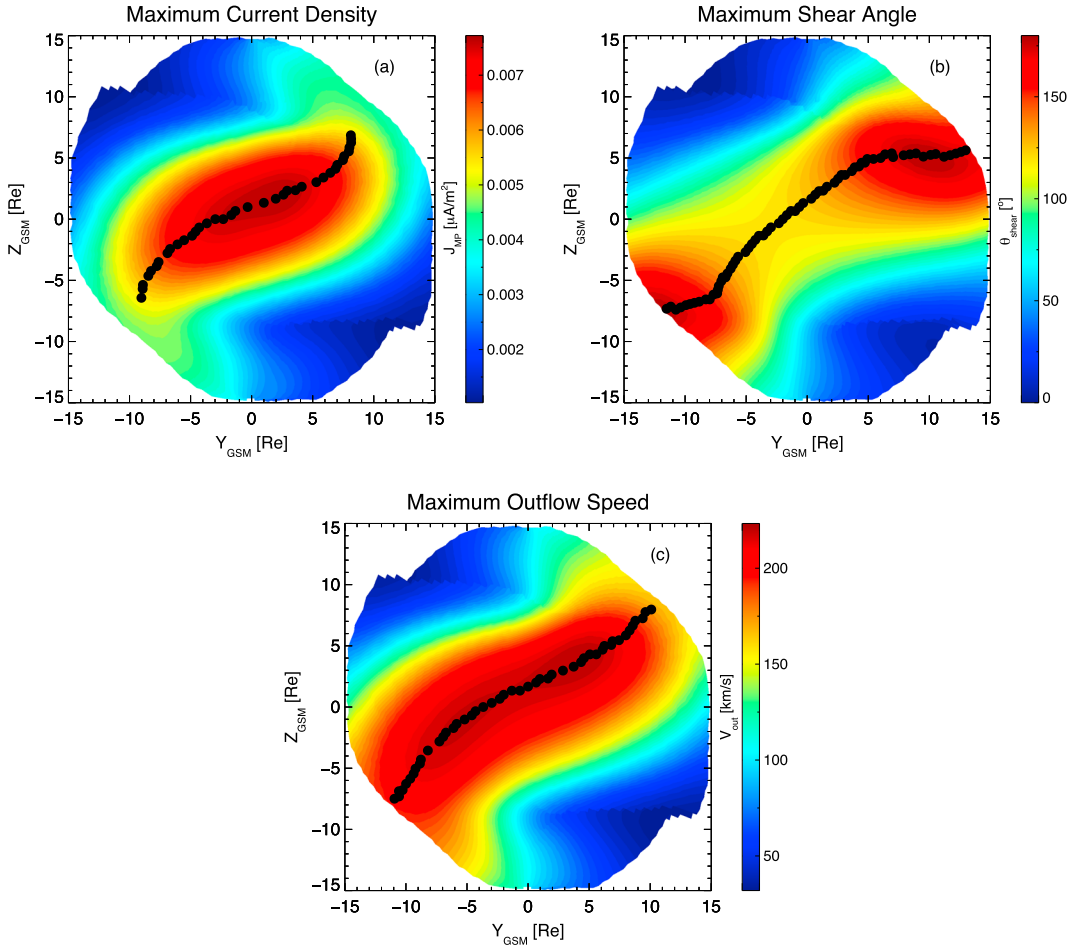

Figure 3. Color coded (a) magnetopause current density magnitude, (b) magnetic shear angle, and (c) asymmetric reconnection outflow velocity along the BATS-R-US dayside magnetopause boundary, as seen in the yz_{GSM} plane. Blank regions denote magnetopause locations where $x_{GSM} < 0$. Each black circle obeys a local maximum condition, as determined by the *Lindeberg* [1993, 1998] ridge-detection algorithm (see text for details). The collection of these points forms the X line location for this configuration. The IMF and Earth's dipole tilt conditions used as input for this BATS-R-US run are $(B_x, B_y, B_z) = (5.0, 5.0, -2.886)$ nT and $\psi = 0°$.

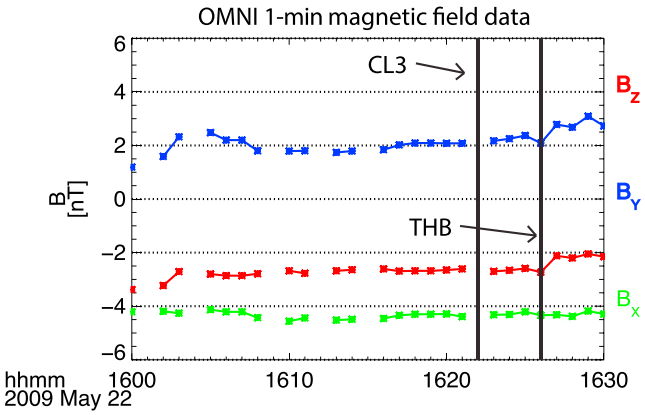

Figure 4. Interplanetary medium's magnetic field data in GSM coordinates for an approximately 20 min interval preceding the quasi-simultaneous reconnection event on 22 May 2009. Cluster 3 (CL3) first cross the dayside magnetopause at 16:22 UT followed by THEMIS B (THB) at 16:26 UT. The representative IMF for this event is obtained as a 20 min average taken prior to one of the spacecraft in the spacecraft pair has crossed the magnetopause which in this case is Cluster 3. The data were provided by the OMNI data set.

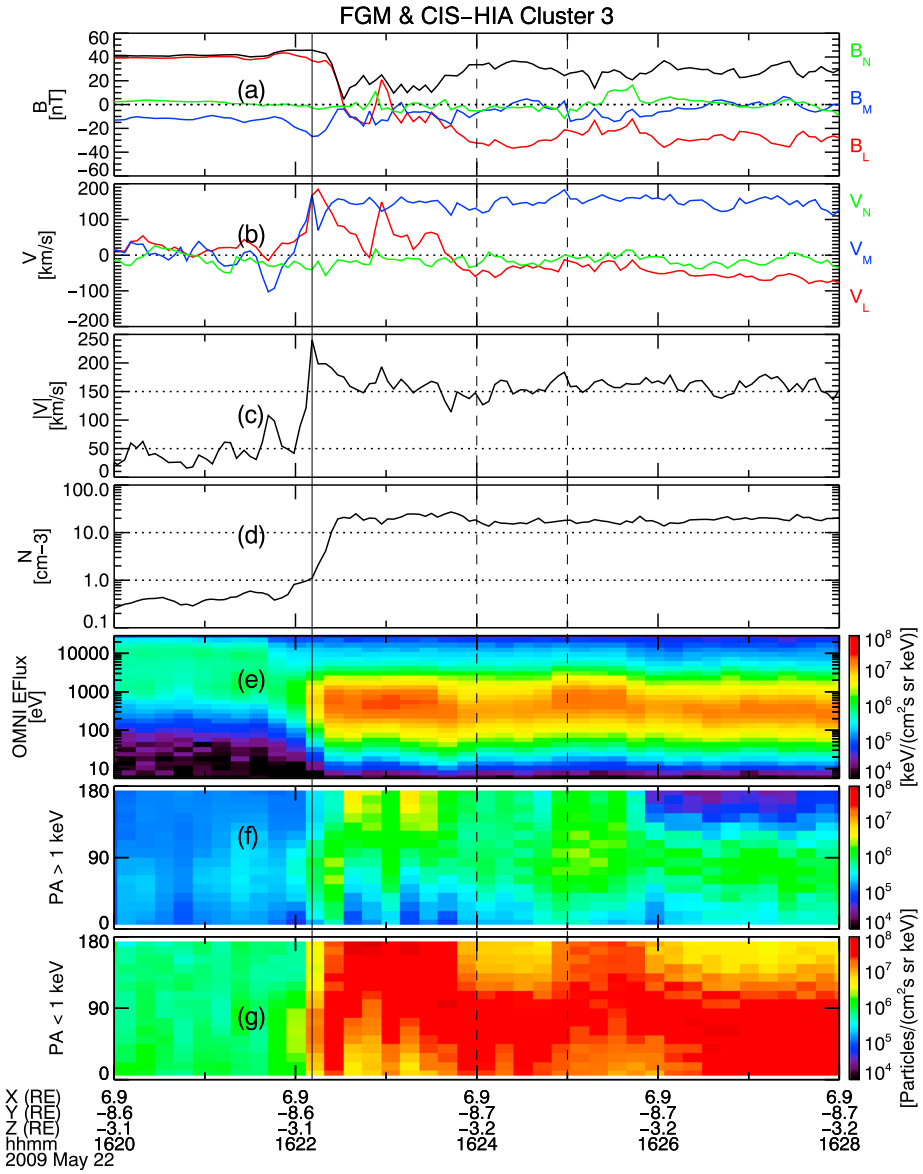

Figure 5. Cluster 3 magnetopause crossing on 22 May 2009 that preceded the quasi-simultaneous THEMIS B magnetopause crossing (see Figure 6). It shows (a) magnetic field and (b) velocity field components in boundary normal coordinates, (c) ion velocity magnitude, (d) ion density, (e) energy-time spectrogram of omnidirectional ion flux, and pitch angle distributions for ion energies (f) above or equal to 1 keV and (g) below 1 keV. The pair of vertical dashed lines and the solid vertical line refer, respectively, to the magnetosheath interval and the maximum outflow velocity, both used in the Walén relation.

the spacecraft pair has crossed the magnetopause. An example of such a procedure is shown in Figure 4. For the three reconnection events analyzed in this section, the IMF was fairly steady for around 20 min, as shown in Figure 4. This is why we have chosen such a long period for averaging out the solar wind parameters.

Each satellite detected accelerated and Alfvénic plasma flows on the magnetospheric side of the magnetopause boundary. For all spacecraft the observed plasma jet magnitude reached more than 50% of the predicted value, i.e., $r_{op} > 0.5$, while the angular displacement from the field-aligned direction was within 30°. All but one spacecraft (Cluster 3) satisfied the criterion $\Delta V_A^* > 0.5$. Besides the flow acceleration detected by Cluster 3 on the magnetospheric side of the magnetopause, there were other reconnection-like signatures present; thus, we still consider that Cluster 3 crossed a reconnecting magnetopause. These other signatures are discussed below, and they are representative of those found in the other two (5 March 2007 and 7 July 2009) events. Figures 5 and 6 show, respectively, Cluster 3 and THEMIS B magnetic field and plasma

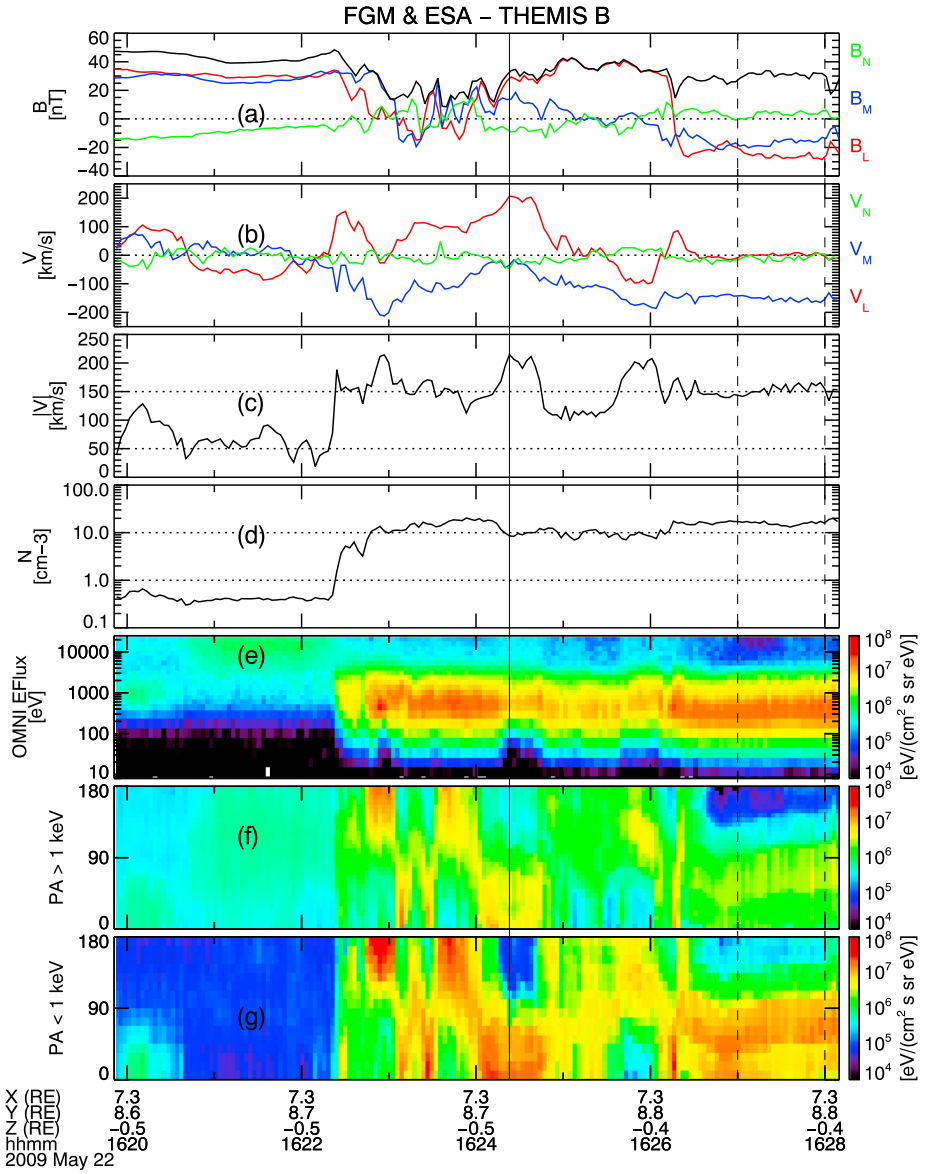

Figure 6. THEMIS B magnetopause crossing on 22 May 2009 that followed the quasi-simultaneous Cluster 3 magnetopause crossing (see Figure 5). Same caption as in Figure 5.

observations for the quasi-simultaneous magnetopause crossing event that occurred on 22 May 2009. Magnetic and velocity field components are presented in boundary normal coordinates *LMN*, where *N* points along the local magnetopause normal, *M* points westward and is identified as the cross product between *N* and z_{GSM} directions, and finally, *L*, which points approximately north, completes the orthogonal system being defined as the cross product between the *M* and *N* vectors [*Russell and Elphic*, 1978]. The boundary normal coordinates, at a given magnetopause location, were obtained by using the *Shue et al.* [1998] magnetopause model. Cluster 3 observations are presented first followed by THEMIS B.

3.1.1. Example of a Quasi-Simultaneous Reconnection Event

Figure 5 shows magnetic field and plasma parameters observed by the Cluster 3 spacecraft during an outbound orbit on 22 May 2009 in the dawn sector of the magnetosphere. Cluster 3 encountered the earthward edge of the magnetopause near 16:22:00 UT. At ~16:22:10 UT, the maximum positive enhancement in the V_L component was detected relative to its negative values in the magnetosheath proper (from 16:26 UT onward). At ~16:23:00 UT, the B_L component changed from magnetospheric ($B_L > 0$) to magnetosheath ($B_L < 0$) magnetic field orientations and the magnetic field magnitude (black line in Figure 5a) reached the

smallest value (~5 nT) for the whole interval shown. Right after that, the B_L component made a brief excursion to positive values while accelerated plasma flows, i.e., a positive enhancement in V_L, were still being measured, suggesting the presence of an acceleration mechanism acting somewhere southward of the spacecraft location. The ion omnidirectional energy flux remained slightly elevated (peak flux ~600 eV), relative to magnetosheath proper levels (peak flux ~300 eV), during the approximately 2 min interval following the main B_L reversal, within which there were accelerated plasma flows. Moreover, within this same 2 min interval, both magnetosheath- and magnetospheric-like ions were streaming antiparallel to the field lines with magnetosheath magnetic field lines orientations ($B_L < 0$), as shown in Figures 5f and 5g. In the context of the reconnection geometry, the antiparallel streaming magnetosheath-like ions could be interpreted as a population which mirrored in the northern ionosphere and returned back to the spacecraft detector along reconnected field lines [*Fuselier et al.*, 1995]. The magnetospheric ions seen on magnetosheath magnetic field lines can be interpreted as escaping ions flowing along field lines "opened" by the reconnection process.

Figure 6 shows that the THEMIS B probe encountered the earthward edge of the magnetopause at ~16:22:25 UT, almost simultaneously with Cluster 3 (16:22:00 UT). THEMIS B has crossed the magnetopause on the dusk sector very close to and below the equator ($z_{GSM} \sim -0.5\ R_E$). It was approximately 16 R_E away from Cluster 3 in the y_{GSM} direction. Upon crossing the earthward edge of the magnetopause, THEMIS B detected accelerated plasma flows, i.e., positive enhancements in both V_L and V_M velocity components at ~16:22:30 UT. Notice that for the latter flow component a positive V_M enhancement is detected as a less negative V_M value when compared to the magnetosheath flow, since the background flow has a negative M (duskward) component, as seen at ~16:22:30 UT and at ~16:24:25 UT. The plasma jet speed was ~240 km/s, corresponding to 64% of the theoretically predicted value. The jet direction was in excellent agreement with theory, i.e., $\theta_{op} = 2.61°$. The ΔV_A^* value was also 0.64. In spite of the lower value found for the ratio of observed to predicted flow speeds, $r_{op} = 0.64$, which in turn might be related to a poor choice of parameters representing local conditions in the reconnection site [*Vines et al.*, 2015], the observed accelerated flows are consistent with the reconnection theory, as well as with the picture where magnetic reconnection was occurring somewhere southward and slightly duskward of the spacecraft's location, with the latter statement based on the local jet direction (northward and slightly dawnward). THEMIS B was in the low-latitude boundary layer (LLBL) at ~ 16:26 UT when Cluster 3 was leaving the magnetosphere at the magnetosheath edge of the magnetopause (~16:25:55 UT).

3.1.2. X Line Location Predictions

Figure 7 presents predicted X line locations (black lines) over the projection of the BATS-R-US dayside magnetopause into the $x_{GSM} = 0$ plane for the three quasi-simultaneous reconnection events described in Table 1. In Figure 7 the 5 March 2007, 22 May 2009, and 7 July 2009 reconnection events correspond to the left, middle, and right columns, respectively. Spacecraft positions at the magnetopause crossing time are overplotted as black circles, as well as the yz_{GSM} projection of the observed reconnection jet direction (red arrows). The figure also shows the expected reconnection jet direction either northward or southward of the X line (black arrows), based on the assumption that the reconnection outflows should be perpendicular to the local X line segment. The IMF and Earth's dipole tilt conditions used as input for the BATS-R-US runs are shown on the top of each panel. Figures 7a–7c show the X line location prediction obtained for the maximum shear angle model [*Trattner et al.*, 2007], while Figures 7d–7f and 7g–7i present the X line location prediction for the maximum magnetopause current density magnitude model and the maximum asymmetric reconnection outflow speed [*Swisdak and Drake*, 2007] model, respectively.

For two reconnection events (Figures 7a, 7d, and 7g and 7b, 7e, and 7h), an extended X line with an east-west (y_{GSM} direction) length of the inter spacecraft separation, i.e., >7 R_E, was able to correctly predict both north-south (V_z) and east-west (V_y) observed jet components. For these two events, both the maximum magnetopause current density and maximum asymmetric reconnection outflow speed models correctly predicted the full yz_{GSM} projection of the observed jets at the two spacecraft locations, while the maximum shear angle model made a full correct prediction only at one event (Figure 7a). For the three reconnection events, the V_z component of the observed jet direction was correctly predicted by all three models at least at one spacecraft location. These results indicate that X lines with lengths of a few R_E can organize reconnection jet observations at far apart locations, although they do not provide any statistical evidence for this.

3.2. Second Set of Reconnection Events: Statistical Analysis

Since the chances for finding events where two (or more) widely separated spacecraft cross a reconnecting magnetopause quasi-simultaneously are very small, we turned to single-spacecraft crossings which, at least

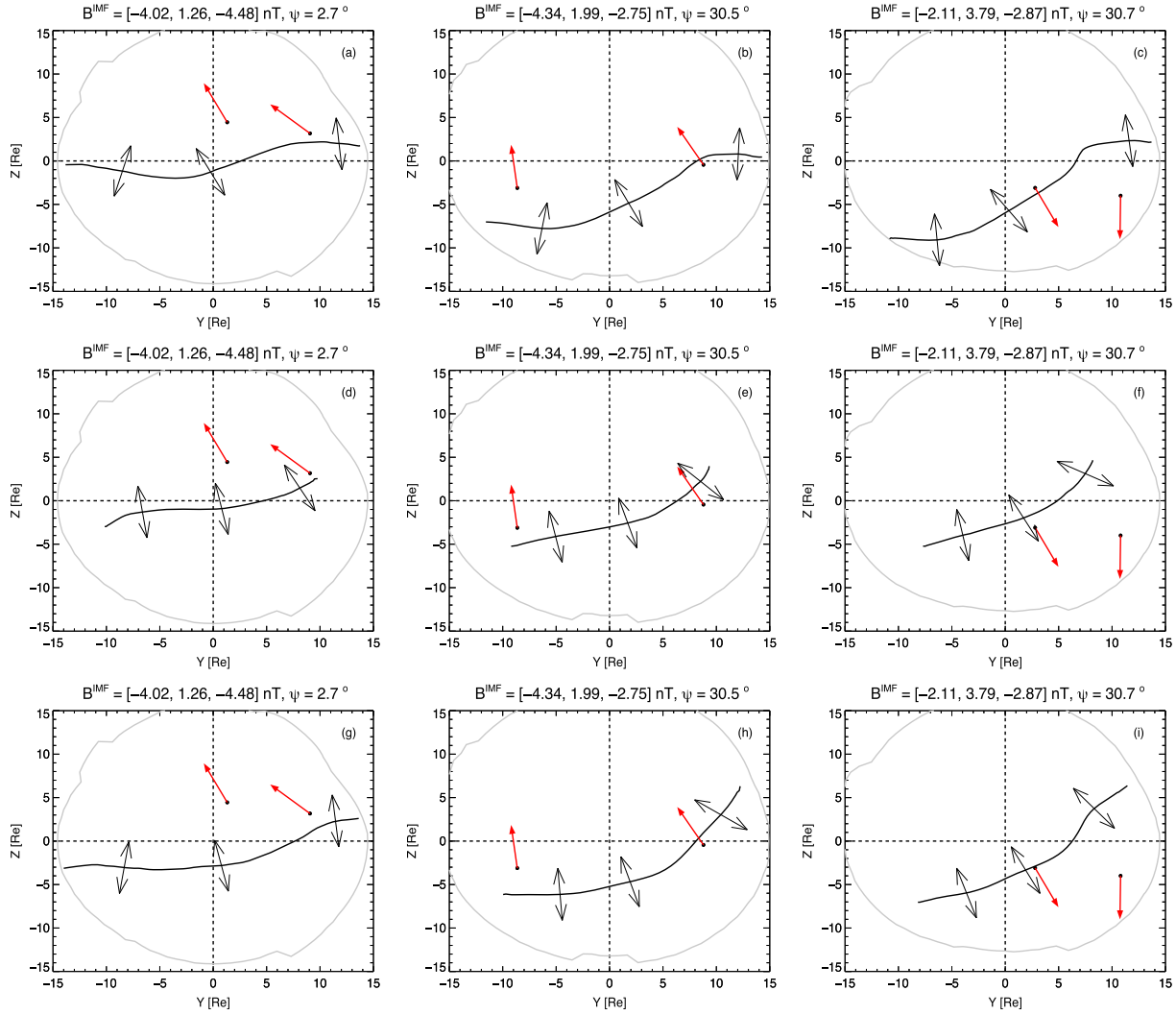

Figure 7. X line model configurations (black lines) as seen in the yz_{GSM} plane for the three quasi-simultaneous reconnection events presented in Table 1. The X line location predictions for (a, d, and g) the 5 March 2007 reconnection event, (b, e, and h) the 22 May 2009 reconnection event, and (c, f, and i) the 7 July 2009 reconnection event. Figures 7a–7c show the results for the *Trattner et al.* [2007] X line model, Figures 7d–7f show the results for the modified component merging model [*Gonzalez and Mozer*, 1974; *Sonnerup*, 1974], and Figures 7g–7i show the results for the *Swisdak and Drake* [2007] model. Earth's dipole tilt (ψ) and IMF conditions for each event are shown on the top of each panel. Black dots represent spacecraft location at the BATS-R-US magnetopause surface and red solid arrows the yz_{GSM} projection of the observed reconnection jet velocity. Black arrows show the expected (locally perpendicular to the X line) reconnection outflow directions for locations both above and below the X line. Gray line indicates the magnetopause surface location at the $x_{GSM} = 0$ plane.

in the case of THEMIS, occur at least twice a day. The goal is to evaluate the performances of the X line models in predicting reconnection jet directions obtained from in situ observations.

First, we looked for solar wind periods where the hourly averaged IMF B_z component observed by ACE was negative for at least 3 h. Then we searched THEMIS magnetopause crossings that occurred during such periods. Moreover, we chose only those crossings where one could clearly see an enhancement in the plasma flow (relative to magnetosheath values) at the earthward (or magnetospheric) side of the magnetopause. The Walén test, as described in section 2.1, was performed for these magnetopause crossings, and we ended up with 75 crossings which have clear reconnection signatures. Such magnetopause crossings were identified as reconnection events. Figure 8 summarizes the ΔV_A^* and θ_{op} parameters found for these 75 events. ΔV_A^* and θ_{op} provide, respectively, a quality measure of the agreement between observed and predicted flow acceleration and the angular displacement of the observed jet direction from the field-aligned direction.

The time period spanned by the THEMIS magnetopause crossings used in this work ranged from May 2007 to March 2013. Figure 9 shows both the yz_{GSM} and xy_{GSM} locations of the 75 THEMIS magnetopause crossings

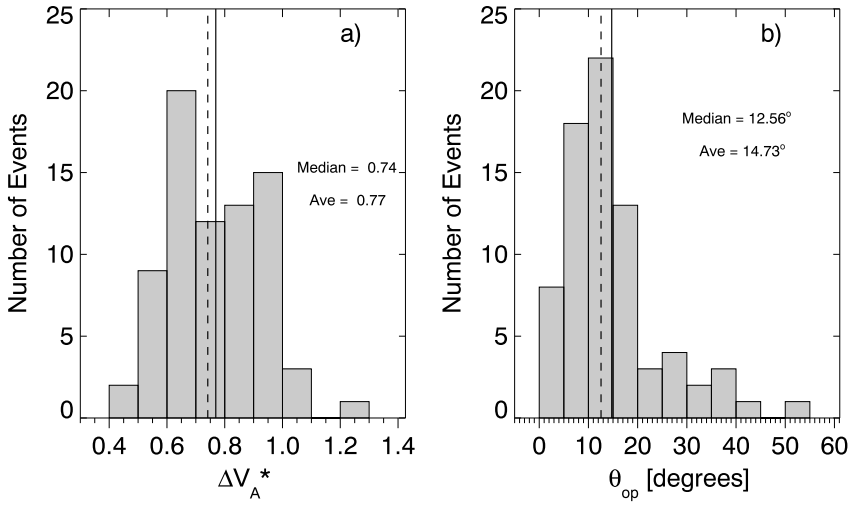

Figure 8. Histogram plots of (a) the quality measure, ΔV_A^*, of the agreement between observed and predicted flow acceleration and (b) the angular displacement, θ_{op}, of the observed jet direction from the field-aligned direction. Both average and median values of the distribution are indicated on each panel. These data refer to 75 THEMIS magnetopause crossing events that occurred between May 2007 and March 2013.

analyzed here. The magnetopause crossing time of each THEMIS probe in this data set is shown in Table 3, along with the IMF conditions. The IMF was obtained either by using the OMNI data set or time-shifting ACE magnetic field data. In what follows, an example of a reconnection event within the THEMIS data survey is shown, as well as a feature that has been used in this work as a further indication that reconnection was occurring.

3.2.1. Example of a Reconnection Event Within the THEMIS Magnetopause Crossing Survey

Figure 10 shows a typical reconnecting magnetopause layer found in our survey. The figure shows a 10 min period of (a) magnetic field and (b) ion velocity components in *LMN* boundary normal coordinates, (c) ion velocity magnitude, (d) ion density, and (e) ion omnidirectional energy flux provided by the THEMIS E spacecraft during an outbound magnetopause crossing on 22 October 2008. Between ~15:42:20 UT and ~15:43:00 UT, THEMIS E first traverses the LLBL, a region where ion density values are between the typical magnetosphere (~0.3 cm^{-3}) and magnetosheath (~10 cm^{-3}) values. A second traversal of the LLBL occurs between ~15:48:00 UT and ~15:49:20 UT. In this region a mixed plasma population constituted by both magnetosphere and magnetosheath particles is present, i.e., ion plasma populations with energies of ~9 keV and ~0.35 keV, respectively.

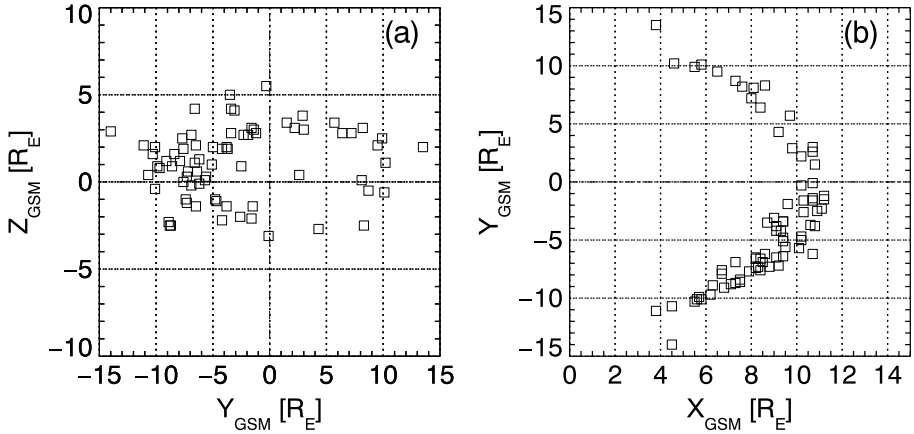

Figure 9. Locations of 75 THEMIS magnetopause crossings at the (a) yz_{GSM} and (b) xy_{GSM} planes. They span the May 2007 to March 2013 period.

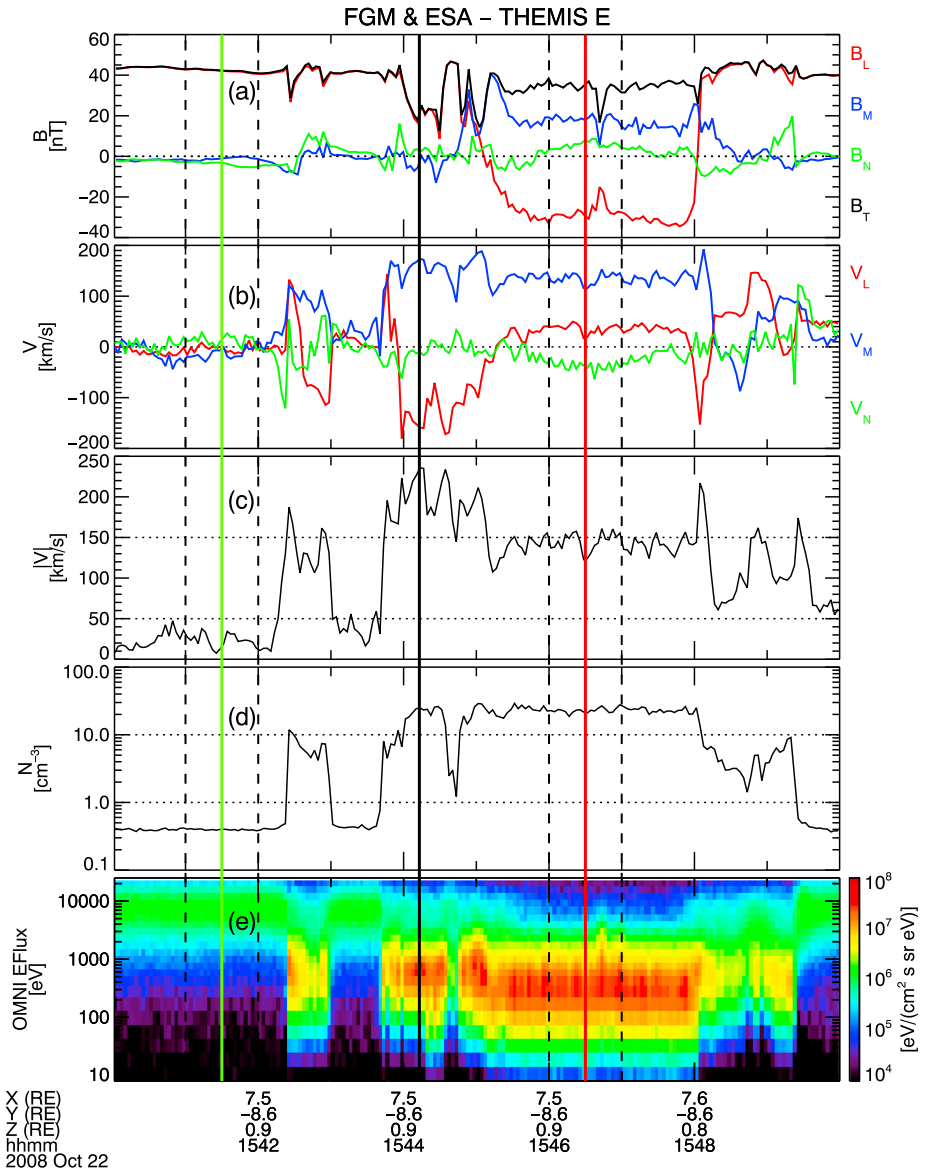

Figure 10. THEMIS E outbound magnetopause crossing on 22 October 2008. Shown are (a) magnetic field strength and components in in situ boundary coordinates, (b) ion velocity in in situ coordinates, (c) ion velocity magnitude, (d) ion density, and (e) energy-time spectra of ion omnidirectional energy flux. The two pairs of vertical dashed lines exemplify the 1 min time intervals from which the magnetosheath (rightmost pair) and magnetosphere (leftmost pair) parameters are averaged out. Magnetosheath and magnetic field and plasma parameters taken at the outflow jet region (vertical black line) are later used in the Walén test. The three vertical solid lines mark instants of time when the ion omnidirectional energy flux data are going to be analyzed into more details in Figure 11.

THEMIS E encountered the magnetopause a number of times before finally exiting the magnetosphere near 16:12:00 UT (not shown). A magnetopause crossing is identified here where the reconnecting component of the magnetic field, B_L, changes sign from magnetospheric ($B_L > 0$) to magnetosheath orientation ($B_L < 0$). In Figure 10, two magnetopause crossings are identified according to this criterion, with the first one occurring near 15:45:10 UT and the second one at ~15:48 UT. We focus on the magnetic field and plasma observations around the first of these magnetopause crossings. At 15:44 UT, the ion plasma speed reaches ~230 km/s corresponding to an increase of ~90 km/s relative to magnetosheath values of ~140 km/s. This local acceleration occurred on the earthward side of the magnetopause where the local magnetic field orientation was mainly northward ($B_L > 0$). The magnetic shear angle θ_{shear} for this crossing was ~148°. The two pairs of vertical dashed lines demarcate the magnetosphere and magnetosheath 1 min time intervals where the magnetic

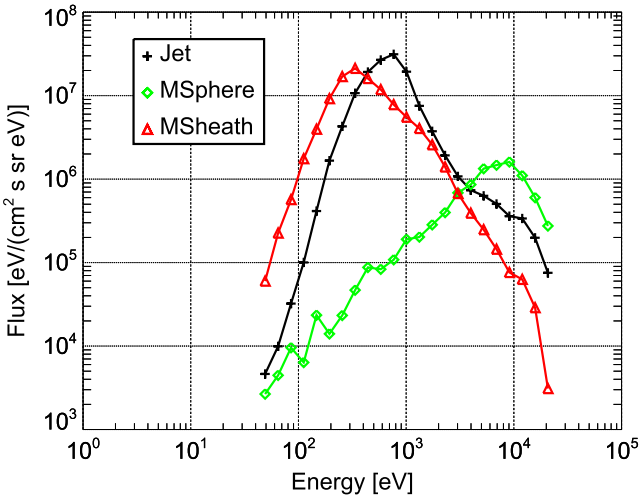

Figure 11. Plot of ion energy flux versus ion energy extracted from the ion omnidirectional energy flux data shown in Figure 10e. Each colored line corresponds to one of the three solid vertical lines in Figure 10e, and they refer to instants of time when the spacecraft was in the magnetosphere (green line, 15:41:30 UT), the plasma jet (black line, 15:43:13 UT), and the magnetosheath (red line, 15:46:30 UT) regions.

field and plasma parameters in each region are averaged. In particular, the averaged magnetosheath parameters and those acquired at the time instant marked by the vertical solid black line are used in the Walén test described in section 2.1. The observed to predicted reconnection outflow ratio was $r_{op} = 0.62$, and the angular displacement of the observed jet from the field-aligned direction was $\theta_{op} = 17°$, providing a $\Delta V_A^* = 0.59$, which is well inside our criterion for a reconnection event.

Figure 11 shows an additional signature consistent with the reconnection interpretation for the observed flow acceleration seen in the example shown here and all the other 74 THEMIS magnetopause crossings in our survey. The three curves of the ion omnidirectional energy flux versus the ion energy are presented as representatives of three different regions shown in Figure 10: the magnetosphere (at 15:41:30 UT, green vertical line), the plasma jet (at 15:44:13 UT, black vertical line) taken at the observed maximum flow speed, and the magnetosheath proper (at 15:46:30 UT, red vertical line). The maximum flux for the plasma jet (black curve) is comparable to that for the magnetosheath (red curve), and both are roughly 1 order of magnitude higher than the highest flux in the magnetosphere (green curve). We emphasize here that the highest ion energy flux in the plasma jet region is at ~800 eV while that in the magnetosheath is at ~350 eV.

The results suggest that magnetosheath particles are crossing the dayside magnetopause and being detected within the magnetosphere, which has been opened by the reconnection process, and in the meantime they are being accelerated and heated. Such an observed plasma acceleration is due to magnetic tension forces acting on the local plasmas which accelerate them as the highly tensioned (reconnected) field lines relax toward a state of minimum energy. The next section describes how the data set was sorted according to IMF orientation and Earth's dipole tilt inclination.

3.2.2. Data Set Separation

Since the 75 THEMIS magnetopause crossings occurred under a variety of IMF and Earth's dipole tilt (ψ) conditions, we decided to separate the data set into representative IMF clock angle ($\theta_{CA} = \tan^{-1}(B_y/B_z)$) and Earth's dipole tilt angle bins. We also took into account the sign of the IMF B_x component when dividing up the data set. The goal is to have a set of representative solar wind and Earth's dipole tilt conditions from which we can derive the X line model locations. Such a set was determined through the following procedure. For either positive or negative IMF B_x component, we would separate the magnetopause crossings into seven equally sized ψ bins of 10° each, with the bin centers ψ_c being ±30°, ±20°, ±10°, and 0°. For each tilt angle bin centered on ψ_c we further separated the magnetopause crossings into five equally sized IMF clock angle bins ranging from 10° to 255°. Each clock angle bin was 30° wide. The clock angle bins centered on θ_{CAc} were 120°, 150°, 180°, 210°, and 240°. We notice that there were events, outside of the 75 THEMIS events used here, for which the IMF clock angle was less than 105° or more than 255°. The representative bins chosen here, however, cover the relevant physics, even though the inputs do not exactly match all the spacecraft measurements.

Table 2. IMF and Earth's Dipole Tilt Values Used as Input for the BATS-R-US Runs in the Statistical Analysis

IMF B_x(nT)		ψ_c				θ_{CAc}					
						120°		150°		180°	
−5	5	0°	10°	20°	30°	B_y (nT)	B_z (nT)	B_y (nT)	B_z (nT)	B_y (nT)	B_z (nT)
						5	−2.886	2.886	−5	0	−5

The IMF B_x, ψ_c, and θ_{CAc} values used as input for the BATS-R-US code are shown in Table 2. For each IMF B_x, ψ_c, and θ_{CAc} combination, an X line model location can be obtained from BATS-R-US outputs as described in section 2.2.4, totaling 24 possible X line configurations for each X line model tested in this study. Notice that these 24 X line configurations refer only to cases when ψ_c is either zero or positive, and θ_{CAc} is less than or equal to 180°. To derive the remaining 12 X line configurations (per X line model) that would encompass the cases when ψ_c is negative and θ_{CAc} is larger than 180°, we invoked symmetry arguments, as follows. When we refer to "obtaining" or "generating" the X line, it means determining the X line (x_{xline}, y_{xline}, and z_{xline}) coordinates, in the GSM system, over the modeled magnetopause surface. Thus, when applying a symmetry argument, we will change the *signs* of either y_{xline} or z_{xline} coordinates of the X line, while the x_{xline} coordinate is left unchanged. For instance, consider an IMF and dipole tilt configuration wherein IMF $B_x = 5$ nT, $\psi_c = 0°$, and $\theta_{CAc} = 120°$ (IMF $B_y = 5$ nT and $B_z = -2.886$ nT). If we keep B_x and ψ_c unchanged, we can argue that the new X line coordinates y_{new} and z_{new} that we would obtain if we had a negative, instead of a positive, B_y, i.e., $\theta_{CAc} = 240°$, would be such that $y_{new} \rightarrow -y_{xline}$ and $z_{new} \rightarrow z_{xline}$. Thus, the z_{GSM} axis can be considered as a symmetry axis for this case. In fact, we can also apply the same symmetry argument for the $\theta_{CAc} = 150°$ case, which will result in the X line for the $\theta_{CAc} = 210°$ case. Another kind of symmetry can also be used where the y_{GSM} axis is the symmetry axis; thus, the relation between the new and old X line coordinates is $y_{new} \rightarrow y_{xline}$ and $z_{new} \rightarrow -z_{xline}$. We use this kind of symmetry when, but not only, $\theta_{CAc} = 180°$, since under these IMF conditions the X line is located nearly parallel to the equator ($z_{GSM} = 0$). Below we summarize all the IMF and dipole tilt combinations for which we have invoked symmetry arguments (left-hand side—LHS) in order to obtain a new set of X line coordinates for another combination of IMF and dipole tilt angle (right-hand side—RHS). The IMF B_z was southward ($B_z < 0$) for all cases.

1. Replace z_{xline} by $-z_{xline}$ while keeping y_{xline} unchanged on the LHS to generate X line coordinates consistent with conditions on the RHS:
   a. $B_x > 0, B_y > 0, \psi \geq 0 \longrightarrow B_x < 0, B_y < 0, \psi < 0$;
   b. $B_x < 0, B_y > 0, \psi \geq 0 \longrightarrow B_x > 0, B_y < 0, \psi < 0$;
   c. $B_x < 0, B_y = 0, \psi \geq 0 \longrightarrow B_x > 0, B_y = 0, \psi < 0$;
   d. $B_x > 0, B_y = 0, \psi \geq 0 \longrightarrow B_x < 0, B_y = 0, \psi < 0$.
2. Replace y_{xline} by $-y_{xline}$ while keeping z_{xline} unchanged on the LHS to generate X line coordinates consistent with conditions on the RHS:
   a. $B_x > 0, B_y > 0, \psi \geq 0 \longrightarrow B_x > 0, B_y < 0, \psi \geq 0$;
   b. $B_x < 0, B_y > 0, \psi \geq 0 \longrightarrow B_x < 0, B_y < 0, \psi \geq 0$;
   c. $B_x > 0, B_y > 0, \psi < 0 \longrightarrow B_x > 0, B_y < 0, \psi < 0$;
   d. $B_x < 0, B_y > 0, \psi < 0 \longrightarrow B_x < 0, B_y < 0, \psi < 0$.

Next, we provide an example illustrating how we use the first kind of symmetry argument presented above. We plotted the X line coordinates in the yz_{GSM} plane as upward triangles in Figure 12 for one of the BATS-R-US runs used in this study where the input IMF and Earth's dipole tilt conditions were (B_x, B_y, B_z) = (+5, +5, −2.886) nT, with a clock angle of $\theta_{CAc} = 120°$ and $\psi_c = +10°$. According to the symmetry argument number 1 mentioned above, if we replace the z_{xline} coordinate by $-z_{xline}$, while keeping the other two coordinates unchanged, the new X line coordinates, i.e., those represented by downward triangles in Figure 12, will be equivalent to the X line coordinates obtained when the BATS-R-US code is run with input IMF and Earth's dipole tilt conditions of (B_x, B_y, B_z) = (−5, −5, −2.886) nT, $\theta_{CAc} = 240°$, and $\psi_c = -10°$. We ran the BATS-R-US code under such conditions, and of course, the solar wind density, velocity, and temperature, as well as the simulation grid setup were kept the same for both runs. The X line coordinates for the run with IMF $B_x = -5$ nT, $\theta_{CAc} = 240°$, and $\psi_c = -10°$ are shown as filled circles in Figure 12. The X line location obtained by using the symmetry argument (downward triangles) and that obtained via the original run (filled circles)

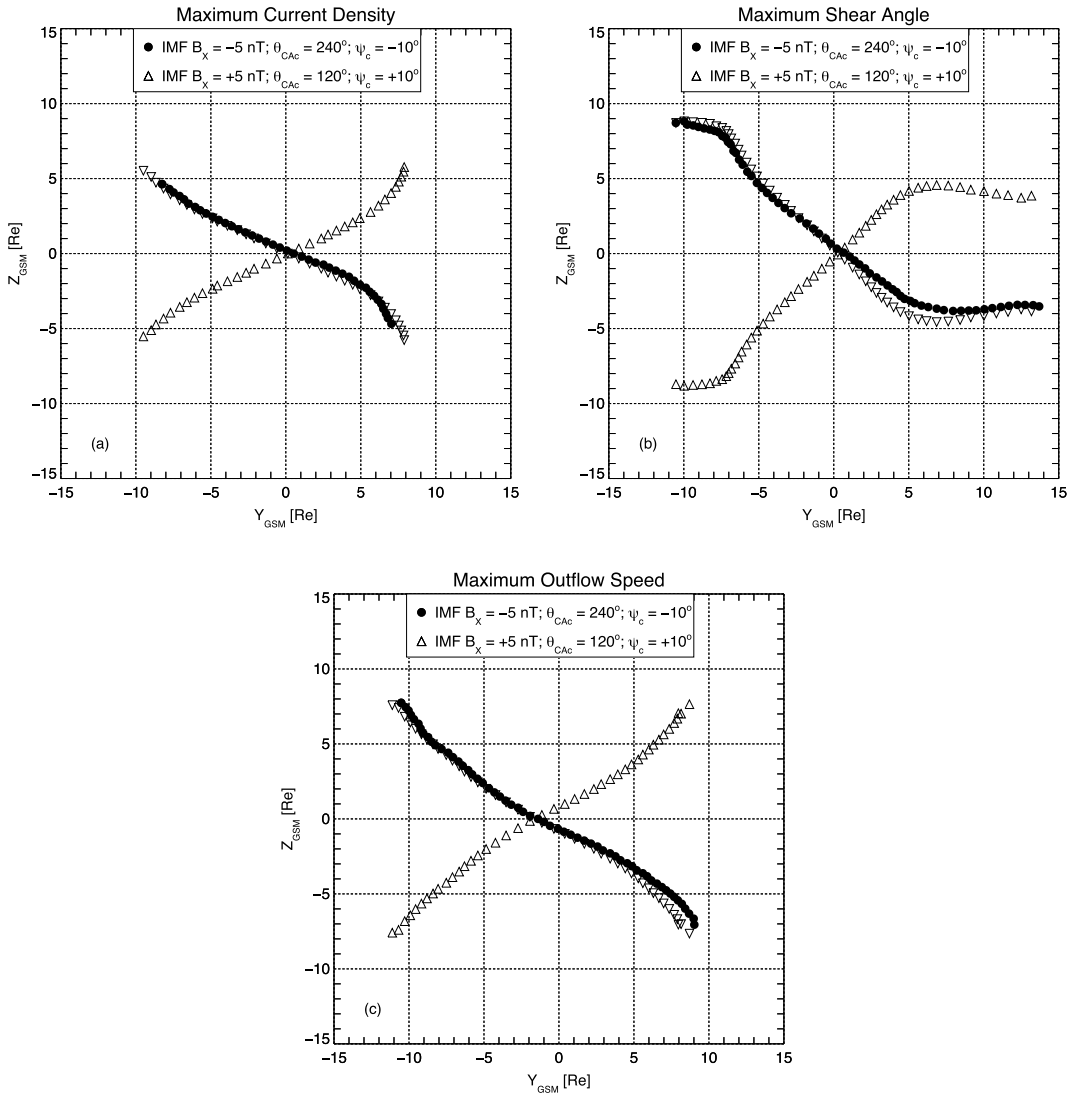

Figure 12. Example of symmetry argument usage for obtaining X line coordinates in global MHD simulations. When replacing the X line GSM coordinates $(x_{\text{xline}}, y_{\text{xline}}, z_{\text{xline}})$ in the IMF $B_x = +5$ nT, $\theta_{\text{CAc}} = 120°$, and $\psi_c = +10°$ run (upward triangles) by $(x_{\text{xline}}, y_{\text{xline}}, -z_{\text{xline}})$, the obtained X line location (downward triangles) is tantamount to obtain the X line location obtained when the BATS-R-US code is run under input IMF and Earth's dipole tilt conditions given by IMF $B_x = -5$ nT, $\theta_{\text{CAc}} = 240°$, and $\psi_c = -10°$ (filled circles).

is essentially on top of each other, for all X line models used, and their locations agree within 1.0 R_E. One can see that the usage of symmetry arguments, as exemplified above, is reasonable and they can be applied in global MHD runs.

3.2.3. Reconnection Jet Direction Predictions and Comparison With In Situ Observations

Here we present our evaluation of each X line model's performance for predicting observed reconnection jet directions. Table 3 summarizes our findings. We demonstrate below the procedure carried out to obtain the features shown in Table 3. Consider, for example, the THEMIS A reconnection event on 14 September 2008, shown in the sixth row of Table 3. The IMF conditions for the event were $(B_x, B_y, B_z) = (-1.6, 2.0, -1.9)$ nT. The Earth's dipole tilt angle obtained from the Geopack (http://ampere.jhuapl.edu/code/idl_geopack.html) package was $\psi = 12.3°$. Taking into account the negative IMF B_x for this case, the IMF clock angle of $\theta_{\text{CA}} \approx 145°$, and the Earth's dipole tilt angle, these parameters fall in the following conditions: IMF $B_x < 0$, $135° < \theta_{\text{CA}} \leq 165°$, and $5° < \psi \leq 15°$. Therefore, the X line models used for this case are those obtained with the following IMF and Earth's dipole tilt conditions used as input for the BATS-R-US run: IMF $B_x = -5$ nT, $\theta_{\text{CAc}} = 150°$, and $\psi_c = 10°$.

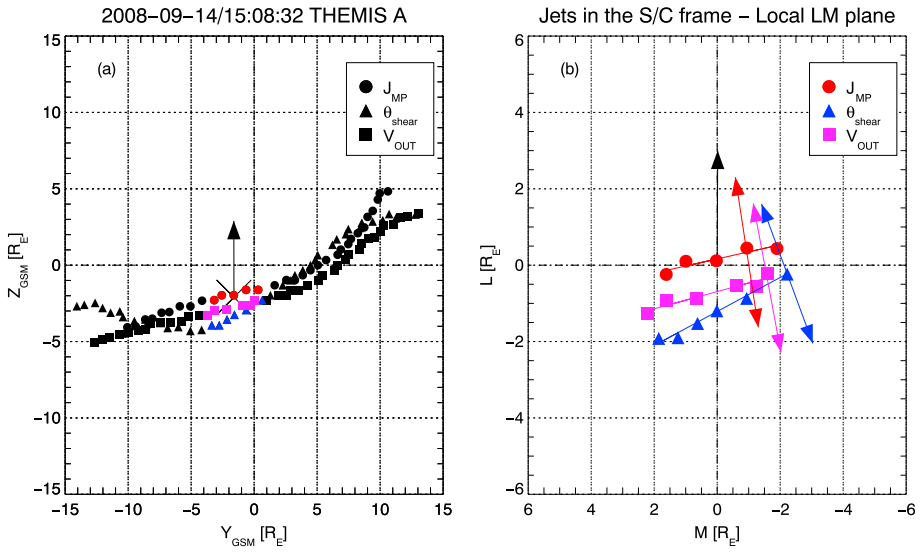

Figure 13. Three X line model locations over the global MHD BATS-R-US' dayside magnetopause during the time period encompassing THEMIS A magnetopause crossing on 14 September 2008. The X line models refer to the maximum magnetopause current density (J_{MP}) model, the maximum shear angle (θ_{shear}) model, and the maximum asymmetric reconnection outflow speed (V_{out}) model. THEMIS A location in Figure 13a is marked by an X sign, and the observed reconnection jet direction projected onto the yz_{GSM} plane is shown as a black arrow. Figure 13b illustrates how the reconnection jet direction prediction test is done. See the text for details.

Figure 13a shows results from the three X line models for the IMF and ψ_c conditions mentioned above. Predictions for the maximum magnetopause current density X line model (J_{MP}) are shown as black circles, while the maximum shear angle (θ_{shear}) and the maximum asymmetric reconnection outflow speed (V_{out}) X line models are shown, respectively, as black triangles and black squares. In Figure 13a, the X line locations are projected onto the yz_{GSM} plane. Additionally, an "X" marks THEMIS A location during its magnetopause crossing. The yz_{GSM} projection of the observed reconnection jet is also overplotted as a black arrow.

To carry out the comparison between the observed jet direction and the predicted jet direction, which in turn is based on the X line location and orientation, we perform a change in reference frame from the center of the Earth to the spacecraft frame, and project both the X line locations and observed jet velocities in the local *LM* plane, which is tangential to the local magnetopause surface. The result of the frame change and velocities rotations is shown in Figure 13b, where the spacecraft position is now in the origin of the *LM* coordinate system, and the black arrow is the observed jet velocity projected onto the local *LM* plane. The colored symbols in Figure 13b represent points pertaining to the X lines shown in Figure 13a. A linear fit of these points (colored lines) represents the X lines orientations in the local *LM* plane. Notice that in order to determine what the local X line orientation would be relative to the spacecraft position, we take only the $(x_{xline}, y_{xline}, z_{xline})$ points whose distance from the spacecraft (x, y, z) location is within 2.5 R_E. The colored symbols shown in Figure 13a are those which satisfy this criterion.

The predicted reconnection jet directions are taken in the direction perpendicular to the local X line orientation in the *LM* plane (colored arrows orthogonal to the respective colored lines in Figure 13b). In the local LM plane, we verify whether each X line model could correctly predict the north-south (*L*) and east-west (*M*) senses of the observed reconnection jet direction. For the case at hand, one can see in Figure 13b that both maximum θ_{shear} and maximum V_{out} X line models could correctly predict the *L* (north-south) component of the observed jet direction, since both X lines are located below the spacecraft location, and therefore, they would predict a northward (+*L*) component of the flow. On the other hand, the *M* (east-west) component of the flow was not correctly predicted by these two models, since the *M* component of the observed flow has a very small negative *M* component, albeit very difficult to see in the figure, while the predicted *M* component should be positive (see blue and magenta upward pointing arrows in Figure 13b). Therefore, for these two models, i.e., maximum θ_{shear} and maximum V_{out}, a checkmark (✓) and an "x" sign would be, respectively,

Table 3. Reconnection Jet Direction Prediction Test for Three X Line Models Using 75 THEMIS Magnetopause Crossings[a]

Event Date / Jet Time / THEMIS Probe		Maximum $\lvert \mathbf{J}_{MP} \rvert$		Maximum θ_{shear}		Maximum V_{out}		IMF (nT)			Input	
		N-S	E-W	N-S	E-W	N-S	E-W	B_x	B_y	B_z	θ_{CAc}	ψ_c
2007-5-11/19:55:56	E	✓	✓	x	x	✓	✓	−2.6	0.3	−0.3	120°	20°
2007-5-17/18:36:00	D	✓	x	✓	x	✓	x	1.5	−3.0	−4.7	210°	30°
2007-5-20/10:15:30	D	✓	✓	✓	✓	✓	✓	−1.6	2.1	−1.6	120°	20°
2008-8-19/16:44:06	D	x	x	✓	✓	x	x	−1.6	−1.6	−2.9	210°	20°
2008-8-31/15:08:43	D	✓	✓	✓	✓	✓	✓	3.1	−2.2	−1.7	240°	20°
2008-9-14/15:08:32	A	?	?	✓	x	✓	x	−1.6	2.0	−2.9	150°	10°
2008-9-14/15:24:48	E	✓	✓	✓	✓	✓	✓	−0.9	0.6	−3.3	180°	10°
2008-9-18/18:03:50	E	?	?	?	?	x	x	−1.0	−0.5	−2.3	180°	10°
2008-9-18/19:57:21	D	✓	✓	✓	✓	✓	✓	0.6	−1.6	−2.0	210°	10°
2008-9-19/16:50:13	E	✓	✓	✓	✓	✓	✓	−1.9	3.4	−1.6	120°	10°
2008-9-19/19:27:34	A	x	✓	?	?	x	✓	1.0	0.6	−2.9	180°	10°
2008-9-25/14:42:13	E	✓	x	✓	✓	✓	x	0.3	−0.8	−2.9	180°	10°
2008-10-12/16:31:32	E	✓	✓	✓	x	✓	✓	−0.5	1.6	−3.6	150°	0°
2008-10-13/08:04:53	A	✓	x	✓	x	✓	x	−3.0	−0.9	−1.8	210°	−10°
2008-10-15/02:14:57	A	x	x	✓	x	?	?	−0.4	1.3	−4.5	150°	−20°
2008-10-15/10:40:58	C	✓	x	✓	x	✓	x	3.0	−2.5	−3.9	150°	−10°
2008-10-19/13:36:35	D	x	x	x	x	x	x	0.3	0.1	−5.4	180°	0°
2008-10-19/23:20:59	A	✓	✓	✓	✓	✓	✓	2.3	−5.4	−2.8	240°	−10°
2008-10-22/15:44:13	E	✓	✓	✓	x	✓	✓	4.4	−2.5	−3.1	210°	0°
2009-5-22/16:24:23	B	x	x	?	?	x	x	−4.3	2.3	−2.7	150°	30°
2009-8-17/18:13:29	E	✓	✓	✓	✓	✓	✓	−0.7	−3.1	−1.9	240°	20°
2009-9-28/22:16:30	D	✓	✓	?	?	✓	✓	−3.9	2.2	−2.0	120°	0°
2009-10-28/14:51:38	A	✓	✓	✓	✓	✓	✓	−2.3	2.7	−1.8	120°	0°
2009-10-31/16:41:59	D	✓	✓	✓	✓	✓	✓	−0.5	0.1	−1.7	180°	0°
2009-11-8/14:09:15	D	x	x	x	✓	x	x	4.1	−2.6	−5.3	210°	−10°
2009-11-14/15:04:24	E	✓	✓	✓	✓	✓	✓	2.3	−6.2	−3.8	240°	−10°
2009-11-14/22:19:33	E	✓	x	✓	x	✓	x	0.1	−2.7	−5.6	210°	−20°
2009-11-26/19:24:29	D	?	?	x	✓	?	?	−5.2	−1.7	−3.2	210°	−10°
2010-11-3/15:24:21	D	✓	✓	✓	✓	✓	✓	−0.9	−1.4	−1.9	150°	−10°
2010-12-4/14:22:16	A	✓	✓	x	x	✓	✓	−2.1	−1.6	−2.2	210°	−10°
2011-10-7/02:56:02	A	x	✓	x	✓	x	✓	−1.1	1.9	−3.5	150°	−10°
2011-10-7/03:33:12	E	✓	✓	✓	x	✓	✓	−1.5	−3.2	−2.4	240°	−10°
2011-12-9/15:33:37	D	✓	✓	✓	✓	✓	✓	2.1	−4.3	−5.5	210°	−10°
2011-12-9/23:28:16	A	✓	x	✓	?	✓	x	5.8	−1.0	−9.5	180°	−20°
2011-12-12/16:08:44	D	✓	✓	✓	✓	✓	✓	−1.1	1.4	−3.9	150°	−10°
2011-12-12/16:20:51	A	✓	✓	✓	✓	✓	✓	−1.1	1.4	−3.9	150°	−10°
2012-1-20/19:46:36	D	✓	x	x	✓	✓	x	−2.7	0.1	−3.5	180°	−10°
2012-2-6/18:41:51	D	✓	✓	✓	x	✓	✓	0.7	−5.5	−4.8	240°	−10°
2012-2-6/18:43:30	A	✓	✓	✓	x	✓	✓	0.7	−5.3	−4.5	240°	−10°
2012-2-6/18:46:54	E	✓	✓	✓	x	✓	✓	0.7	−5.3	−4.5	240°	−10°
2012-2-10/18:55:10	A	✓	✓	✓	x	✓	✓	−1.6	2.5	−3.2	150°	−10°
2012-2-15/16:54:49	A	✓	✓	✓	✓	✓	✓	2.5	−7.1	−4.9	240°	0°
2012-2-15/17:38:54	E	✓	✓	✓	x	✓	✓	1.2	−4.1	−7.3	210°	0°
2012-2-15/17:45:42	D	?	?	✓	✓	x	x	−0.3	−1.5	−8.4	180°	0°
2012-11-11/09:55:11	A	✓	✓	✓	x	✓	✓	−0.8	−4.6	−1.9	240°	−20°
2012-11-20/03:17:34	A	x	x	x	x	x	x	0.5	−3.4	−5.3	210°	−30°

Table 3. (continued)

Event Date / Jet Time / THEMIS Probe		Maximum $\lvert \mathbf{J}_{MP} \rvert$		Maximum θ_{shear}		Maximum V_{out}		IMF (nT)			Input	
		N-S	E-W	N-S	E-W	N-S	E-W	B_x	B_y	B_z	θ_{CAc}	ψ_c
2012-11-20/18:55:20	E	✓	x	?	?	✓	x	−1.2	−1.3	−6.7	180°	−10°
2012-11-20/21:00:06	E	x	✓	✓	✓	x	x	2.2	1.5	−6.8	180°	−20°
2012-12-10/02:07:37	D	✓	✓	✓	?	✓	✓	−1.2	−2.7	−2.9	210°	−30°
2012-12-13/02:39:26	D	?	?	x	?	?	?	1.8	4.7	−3.3	120°	−30°
2012-12-13/20:45:23	E	✓	x	✓	x	✓	x	−1.6	1.5	−2.9	150°	−20°
2012-12-23/11:37:27	E	?	?	✓	x	✓	x	−2.1	0.5	−2.5	180°	−20°
2012-12-26/10:58:56	E	x	x	?	?	x	x	0.5	−3.7	−4.2	210°	−20°
2013-1-2/08:01:08	A	x	x	✓	✓	x	x	−1.2	2.0	−3.6	150°	−30°
2013-1-2/22:12:54	D	✓	x	x	✓	✓	x	−1.6	−1.6	−2.4	210°	−20°
2013-1-14/15:25:39	E	✓	x	✓	x	✓	x	−1.0	−0.7	−3.6	180°	−10°
2013-1-20/03:42:07	D	?	?	✓	✓	✓	✓	2.0	3.9	−5.0	150°	−30°
2013-1-20/06:58:12	E	x	x	✓	✓	✓	✓	3.7	4.7	−6.2	150°	−30°
2013-1-21/06:37:11	D	?	?	x	x	?	?	−0.7	−2.3	−2.6	210°	−30°
2013-1-23/03:01:11	D	✓	✓	✓	✓	✓	✓	−1.6	−0.5	−2.1	180°	−30°
2013-1-23/08:34:43	E	✓	x	✓	x	✓	x	1.7	1.5	−1.2	120°	−30°
2013-1-31/22:02:05	A	✓	x	✓	x	✓	x	−2.9	1.4	−4.0	150°	−10°
2013-2-5/23:17:13	A	x	x	?	?	x	x	−1.4	2.9	−1.4	120°	−20°
2013-2-11/04:15:25	D	✓	x	✓	x	✓	x	−3.7	−0.5	−2.1	180°	−20°
2013-2-13/01:42:54	E	✓	✓	✓	✓	✓	✓	−1.3	−2.1	−4.5	210°	−20°
2013-2-14/06:10:03	A	✓	✓	✓	x	✓	✓	−0.6	3.2	−6.9	150°	−20°
2013-2-15/02:45:20	D	x	x	x	x	x	x	−2.8	1.4	−1.0	120°	−20°
2013-2-17/17:29:30	D	✓	✓	✓	✓	✓	✓	1.9	2.2	−6.2	150°	0°
2013-2-22/12:27:26	D	✓	✓	✓	x	✓	✓	0.3	−3.9	−3.7	240°	−10°
2013-2-22/20:51:05	A	x	x	x	x	x	x	0.1	−4.1	−3.8	240°	0°
2013-2-24/14:52:47	D	x	x	x	✓	x	x	2.7	−0.8	−2.2	210°	0°
2013-3-8/22:34:35	D	✓	x	✓	x	✓	x	0.3	−0.1	−0.7	180°	0°
2013-3-8/22:58:21	D	?	?	x	x	✓	✓	0.3	1.7	−2.2	150°	0°
2013-3-8/23:19:37	E	✓	✓	✓	✓	✓	✓	−1.4	0.5	−2.1	180°	−10°
2013-3-23/12:46:42	A	✓	✓	✓	x	✓	✓	2.9	−3.0	−2.5	240°	10°
		Total N-S	Total E-W	Total N-S	Total E-W	Total N-S	Total E-W					
		50	38	53	32	55	40					

[a]The ✓(x) symbol indicates that a given X line model (in)correctly predicted either the north-south (N-S) or east-west (E-W) senses of the observed plasma jet direction. Question mark (?) symbols refer to unclear predictions (see text for details). The IMF clock angle (θ_{CAc}) and the Earth's dipole tilt (ψ_c) conditions used as input for deriving the X line model locations via global MHD simulations are also shown.

Table 4. Summary of X line Model Performances on Predicting the North-South (N-S) and East-West (E-W) Senses of Observed Reconnection Jet Directions in 75 THEMIS Magnetopause Crossing Events

X Line Model	Correct N-S Predictions	Correct E-W Predictions
Maximum magnetopause current density	50 (66%)	38 (50%)
Maximum magnetic shear angle	53 (70%)	32 (42%)
Maximum asymmetric reconnection outflow speed	55 (73%)	40 (53%)

placed under the N-S (north-south) and E-W (east-west) columns of Table 3, meaning that these two X line models could (in)correctly predict the north-south (east-west) component of the reconnection jet direction observed by THEMIS A on 14 September 2008 during an outbound magnetopause crossing.

We now discuss what would be the maximum J_{MP} X line jet direction prediction for this reconnection event. Notice that both the X line and spacecraft locations coincide. We established that whenever the minimum distance between the spacecraft location and the local X line segment in the *LM* plane is within 1.0 R_E, which we defined to be the uncertainty in the model X line location, we argue that the X line model cannot provide a clear prediction of the reconnection jet direction, and then a question mark (?) is placed under both N-S and E-W columns of Table 3.

We follow the aforementioned procedure to all THEMIS reconnection events, and the results for the jet direction prediction test can be viewed in Table 3 for each magnetopause crossing. When we sum the number of events that each X line model correctly predicted the north-south (east-west) sense of the observed jet direction, the results shown in Table 4 are found.

4. Summary and Discussion

In this work, we performed an intercomparison of three analytical models which predict both the location and orientation of the large-scale reconnection X line along the Earth's dayside magnetopause, namely, the maximum shear angle model [*Trattner et al.*, 2007], the maximum magnetopause current density magnitude model, which was referred to as a modified version of the standard component merging model [*Gonzalez and Mozer*, 1974; *Sonnerup*, 1974], and the maximum asymmetric reconnection outflow speed model [*Swisdak and Drake*, 2007]. Specifically, we investigated which X line model would correctly predict the north-south and east-west senses of in situ observations of accelerated, nearly field-aligned plasma flows, also known as reconnection jets.

We used two sets of reconnection events to carry out our study. The first of them showed three fortuitous events where two widely (>7 R_E) separated spacecraft crossed the dayside magnetopause quasi-simultaneously during periods of magnetic reconnection. Each spacecraft detected reconnection jets on the earthward side of the magnetopause boundary. For two events the modified component merging model and the *Swisdak and Drake* [2007] model agree with the expected X line location at both spacecraft locations, and for all events one reconnection jet has either its north-south or east-west component correctly predicted by all X line models. Although not possessing a meaningful statistical significance, the results of the first set of reconnection events indicated that X lines several R_E long can organize reconnection jet observations at locations far apart.

Turning to the second set of reconnection events, we gathered 75 THEMIS magnetopause crossings where a single spacecraft crossed the dayside magnetopause boundary. Clear reconnection jets as well as other reconnection-related characteristics attended all these THEMIS crossings. Our results showed that the *Swisdak and Drake* [2007] X line model correctly predicted 73% (53%) of the north-south (east-west) sense of the observed jet directions, while the *Trattner et al.* [2007] and the modified component merging model [*Gonzalez and Mozer*, 1974; *Sonnerup*, 1974] correctly predicted the north-south (east-west) sense of the observed jet directions in 70% (32%) and 66% (38%) of the cases, respectively. We note that the number of correct east-west predictions was always less than the north-south predictions. The main cause for such a discrepancy is that even with the magnetosheath flow component subtracted from the observed accelerated flow, the resultant jet directions, in some cases, are not always in the expected east-west sense which in turn is derived by the knowledge of the observed sign of the IMF B_y component. For instance, for a positive IMF B_y with the spacecraft detecting a plasma jet above (below) the reconnection X line, a negative (positive) y_{GSM} jet component would be expected. As a result, the representative X line trace could not provide a correct prediction of the jet's east-west component, except in cases where the X line geometry possessed some curvature in such a way that it would correctly predict the jet's east-west sense.

It is emphasized here that any of the X line models used in this work provides a prediction of the resultant reconnection outflow direction. The *Swisdak and Drake* [2007] model, for instance, addresses only the reconnection outflow *magnitude*. The jet direction predictions were based on the simple assumption that the reconnection flows leave the X line in a direction perpendicular to the local X line segment, as predicted by standard reconnection theories [see, e.g., *Vasyliunas*, 1975]. In fact, reconnection flows need not be perpendicular to the reconnection line, and their directions are controlled by local plasma and magnetic field

conditions. The simple illustrative model of boundary layer plasma flow of *Cowley and Owen* [1989] exemplifies this matter, in particular their bottom right panels of Figures 5a–5d. Nonetheless, one can verify that the flows certainly maintain their original directions far from the reconnection line, although they are not strictly perpendicular to the reconnection line. Hence, our usage of the simplifying assumption of locally perpendicular flows seems to be justified, at least to a first-order approximation.

Our statistical analysis showed that there is not a significant difference in the performance of the X line models analyzed in this study for the position of the X line. There is a slight tendency, though, for the *Swisdak and Drake* [2007] X line model to better fit the observational data set in an overall sense. Unlike the other two X line models, the *Swisdak and Drake* [2007] model takes into account the realistic asymmetric magnetic fields and plasma density conditions across the magnetopause boundary layer. Perhaps this characteristic might have been the key for the slightly better results of the *Swisdak and Drake* [2007] X line model in our data set. If that is the case, one might argue that local, in addition to external, boundary conditions may play an important role in determining the large-scale X line location. However, our results are not conclusive in this respect.

Acknowledgments
This work was funded by the São Paulo Research Foundation (FAPESP) grants 2014/21229-9 and 2015/20104-0. B. Walsh was supported through NASA grants NNX16AJ73G and NNX16AD91G. D. Koga thanks the National Council for Research and Development (CNPq) PDS program grant 112886/2015-9 for the financial support. The authors thank the University of Michigan's Center for Space Environment Modeling (CSEM at http://csem.engin.umich.edu/) for providing the BATS-R-US code and the Community Coordinated Modeling Center (CCMC) at NASA/Goddard Space Flight Center for running the BATS-R-US code. The authors are indebted with the THEMIS, Cluster, Double Star TC-1, and ACE teams for providing high-quality science data for the Space Physics community. THEMIS data are freely available, and they can be both downloaded and manipulated by using the Space Physics Environment Data Analysis Software (SPEDAS) at http://themis.ssl.berkeley.edu/software.shtml.

References

Alexeev, I. I., D. G. Sibeck, and S. Y. Bobrovnikov (1998), Concerning the location of magnetopause merging as a function of the magnetopause current strength, *J. Geophys. Res.*, *103*(A4), 6675–6684, doi:10.1029/97JA02863.

Angelopoulos, V., et al. (2008), Tail reconnection triggering substorm onset, *Science*, *321*(5891), 931–935, doi:10.1126/science.1160495.

Auster, H., et al. (2008), The THEMIS Fluxgate Magnetometer, *Space Sci. Rev.*, *141*(1–4), 235–264, doi:10.1007/s11214-008-9365-9.

Balogh, A., et al. (2001), The Cluster magnetic field investigation: Overview of in-flight performance and initial results, *Ann. Geophys.*, *19*(10–12), 1207–1217, doi:10.5194/angeo-19-1207-2001.

Carr, C., et al. (2005), The Double Star magnetic field investigation: Instrument design, performance and highlights of the first year's observations, *Ann. Geophys.*, *23*(8), 2713–2732, doi:10.5194/angeo-23-2713-2005.

Cooling, B. M. A., C. J. Owen, and S. J. Schwartz (2001), Role of the magnetosheath flow in determining the motion of open flux tubes, *J. Geophys. Res.*, *106*, 18,763–18,776, doi:10.1029/2000JA000455.

Cowley, S., and C. Owen (1989), A simple illustrative model of open flux tube motion over the dayside magnetopause, *Planet. Space Sci.*, *37*(11), 1461–1475, doi:10.1016/0032-0633(89)90116-5.

Crooker, N. U. (1979), Dayside merging and cusp geometry, *J. Geophys. Res.*, *84*(A3), 951–959, doi:10.1029/JA084iA03p00951.

Dunlop, M. W., et al. (2011), Extended magnetic reconnection across the dayside magnetopause, *Phys. Rev. Lett.*, *2*, 025004, doi:10.1103/PhysRevLett.107.025004.

Escoubet, C. P., M. Fehringer, and M. Goldstein (2001), The Cluster mission, *Ann. Geophys.*, *19*(10–12), 1197–1200, doi:10.5194/angeo-19-1197-2001.

Fazakerley, A. N., et al. (2005), The Double Star Plasma Electron and Current Experiment, *Ann. Geophys.*, *23*(8), 2733–2756, doi:10.5194/angeo-23-2733-2005.

Fuselier, S. A., B. J. Anderson, and T. G. Onsager (1995), Particle signatures of magnetic topology at the magnetopause: AMPTE/CCE observations, *J. Geophys. Res.*, *100*(A7), 11,805–11,821, doi:10.1029/94JA02811.

Fuselier, S. A., K. J. Trattner, and S. M. Petrinec (2011), Antiparallel and component reconnection at the dayside magnetopause, *J. Geophys. Res.*, *116*, A10227, doi:10.1029/2011JA016888.

Gonzalez, W. D., and F. S. Mozer (1974), A quantitative model for the potential resulting from reconnection with an arbitrary interplanetary magnetic field, *J. Geophys. Res.*, *79*(28), 4186–4194.

Hoilijoki, S., V. M. Souza, B. M. Walsh, P. Janhunen, and M. Palmroth (2014), Magnetopause reconnection and energy conversion as influenced by the dipole tilt and the IMF B_x, *J. Geophys. Res. Space Physics*, *119*, 4484–4494, doi:10.1002/2013JA019693.

Hudson, P. D. (1970), Discontinuities in an anisotropic plasma and their identification in the solar wind, *Planet. Space Sci.*, *18*, 1611–1622, doi:10.1016/0032-0633(70)90036-X.

King, J. H., and N. E. Papitashvili (2005), Solar wind spatial scales in and comparisons of hourly Wind and ACE plasma and magnetic field data, *J. Geophys. Res.*, *110*, A02104, doi:10.1029/2004JA010649.

Komar, C. M., P. A. Cassak, J. C. Dorelli, A. Glocer, and M. M. Kuznetsova (2013), Tracing magnetic separators and their dependence on IMF clock angle in global magnetospheric simulations, *J. Geophys. Res. Space Physics*, *118*, 4998–5007, doi:10.1002/jgra.50479.

Komar, C. M., R. L. Fermo, and P. A. Cassak (2015), Comparative analysis of dayside magnetic reconnection models in global magnetosphere simulations, *J. Geophys. Res. Space Physics*, *120*, 276–294, doi:10.1002/2014JA020587.

Laitinen, T. V., M. Palmroth, T. I. Pulkkinen, P. Janhunen, and H. E. J. Koskinen (2007), Continuous reconnection line and pressure-dependent energy conversion on the magnetopause in a global MHD model, *J. Geophys. Res.*, *112*, A11201, doi:10.1029/2007JA012352.

Lindeberg, T. (1993), Discrete derivative approximations with scale-space properties: A basis for low-level feature extraction, *J. Math. Imaging Vision*, *3*(4), 349–376.

Lindeberg, T. (1998), Edge detection and ridge detection with automatic scale selection, *Int. J. Comput. Vision*, *30*(2), 117–156.

Liu, Z. X., C. P. Escoubet, Z. Pu, H. Laakso, J. K. Shi, C. Shen, and M. Hapgood (2005), The Double Star mission, *Ann. Geophys.*, *23*(8), 2707–2712, doi:10.5194/angeo-23-2707-2005.

Luhmann, J. G., R. J. Walker, C. T. Russell, N. U. Crooker, J. R. Spreiter, and S. S. Stahara (1984), Patterns of potential magnetic field merging sites on the dayside magnetopause, *J. Geophys. Res.*, *89*(A3), 1739–1742, doi:10.1029/JA089iA03p01739.

McFadden, J., C. Carlson, D. Larson, M. Ludlam, R. Abiad, B. Elliott, P. Turin, M. Marckwordt, and V. Angelopoulos (2008), The THEMIS ESA plasma instrument and in-flight calibration, *Space Sci. Rev.*, *141*(1–4), 277–302, doi:10.1007/s11214-008-9440-2.

Moore, T. E., M.-C. Fok, and M. O. Chandler (2002), The dayside reconnection X line, *J. Geophys. Res.*, *107*(A10), 1332, doi:10.1029/2002JA009381.

Paschmann, G., M. Øieroset, and T. D. Phan (2013), In-situ observations of reconnection in space, *Space Sci. Rev.*, *178*(2–4), 385–417, doi:10.1007/s11214-012-9957-2.

Phan, T., et al. (2001), Evidence for an extended reconnection line at the dayside magnetopause, *Earth Planets Space*, *53*(6), 619–625, doi:10.1186/BF03353281.

Phan, T. D., et al. (2000), Extended magnetic reconnection at the Earth's magnetopause from detection of bi-directional jets, *Nature*, *404*(6780), 848–850.
Phan, T. D., et al. (2006), A magnetic reconnection X-line extending more than 390 Earth radii in the solar wind, *Nature*, *439*, 175–178, doi:10.1038/nature04393.
Phan, T. D., G. Paschmann, J. T. Gosling, M. Oieroset, M. Fujimoto, J. F. Drake, and V. Angelopoulos (2013), The dependence of magnetic reconnection on plasma beta and magnetic shear: Evidence from magnetopause observations, *Geophys. Res. Lett.*, *40*, 11–16, doi:10.1029/2012GL054528.
Pinnock, M., G. Chisham, I. J. Coleman, M. P. Freeman, M. Hairston, and J.-P. Villain (2003), The location and rate of dayside reconnection during an interval of southward interplanetary magnetic field, *Ann. Geophys.*, *21*(7), 1467–1482, doi:10.5194/angeo-21-1467-2003.
Pu, Z. Y., et al. (2007), Global view of dayside magnetic reconnection with the dusk-dawn IMF orientation: A statistical study for Double Star and Cluster data, *Geophys. Res. Lett.*, *34*, L20101, doi:10.1029/2007GL030336.
Réme, H., et al. (2001), First multispacecraft ion measurements in and near the Earth's magnetosphere with the identical Cluster ion spectrometry (CIS) experiment, *Ann. Geophys.*, *19*(10–12), 1203–1354, doi:10.5194/angeo-19-1303-2001.
Réme, H., et al. (2005), The HIA instrument on board the Tan Ce 1 Double Star near-equatorial spacecraft and its first results, *Ann. Geophys.*, *23*(8), 2757–2774, doi:10.5194/angeo-23-2757-2005.
Russell, C. T., and R. C. Elphic (1978), Initial ISEE magnetometer results: Magnetopause observations, *Space Sci. Rev.*, *22*, 681–715, doi:10.1007/BF00212619.
Scurry, L., C. T. Russell, and J. T. Gosling (1994), A statistical study of accelerated flow events at the dayside magnetopause, *J. Geophys. Res.*, *99*(A8), 14,815–14,829, doi:10.1029/94JA00793.
Semenov, V. S., and M. I. Pudovkin (1985), Localization and features of the development of reconnection processes at the magnetopause, *Geomagn. Aeron.*, *25*, 592–597.
Shue, J.-H., et al. (1998), Magnetopause location under extreme solar wind conditions, *J. Geophys. Res.*, *103*, 17,691–17,700, doi:10.1029/98JA01103.
Sibeck, D., et al. (1999), Plasma transfer processes at the magnetopause, *Space Sci. Rev.*, *88*(1–2), 207–283, doi:10.1023/A:1005255801425.
Sibeck, D. G., and R.-Q. Lin (2011), Concerning the motion and orientation of flux transfer events produced by component and antiparallel reconnection, *J. Geophys. Res.*, *116*, A07206, doi:10.1029/2011JA016560.
Sonnerup, B. U. Ö. (1974), Magnetopause reconnection rate, *J. Geophys. Res.*, *79*(10), 1546–1549, doi:10.1029/JA079i010p01546.
Souza, V. M. (2015), Location of large scale reconnection at Earth's dayside magnetopause as probed by analytical X-line models and in situ observations, PhD thesis, Natl. Inst. for Space Res., São José dos Campos, São Paulo, Brazil.
Stone, E., A. Frandsen, R. Mewaldt, E. Christian, D. Margolies, J. Ormes, and F. Snow (1998), The Advanced Composition Explorer, *Space Sci. Rev.*, *86*(1–4), 1–22, doi:10.1023/A:1005082526237.
Swisdak, M., and J. F. Drake (2007), Orientation of the reconnection X-line, *Geophys. Res. Lett.*, *34*, L11106, doi:10.1029/2007GL029815.
Swisdak, M., B. N. Rogers, J. F. Drake, and M. A. Shay (2003), Diamagnetic suppression of component magnetic reconnection at the magnetopause, *J. Geophys. Res. Space Physics*, *108*(A5), 1218, doi:10.1029/2002JA009726.
Swisdak, M., M. Opher, J. F. Drake, and F. A. Bibi (2010), The vector direction of the interstellar magnetic field outside the heliosphere, *Astrophys. J.*, *710*(2), 1769.
Tóth, G., et al. (2011), Adaptive numerical algorithms in space weather modeling, *J. Comput. Phys.*, *231*(3), 870–903, doi:10.1016/j.jcp.2011.02.006.
Trattner, K. J., J. S. Mulcock, S. M. Petrinec, and S. A. Fuselier (2007), Probing the boundary between antiparallel and component reconnection during southward interplanetary magnetic field conditions, *J. Geophys. Res.*, *112*, A08210, doi:10.1029/2007JA012270.
Trattner, K. J., S. M. Petrinec, S. A. Fuselier, and T. D. Phan (2012), The location of reconnection at the magnetopause: Testing the maximum magnetic shear model with THEMIS observations, *J. Geophys. Res.*, *117*, A01201, doi:10.1029/2011JA016959.
Trenchi, L., et al. (2008), Occurrence of reconnection jets at the dayside magnetopause: Double Star observations, *J. Geophys. Res.*, *113*, A07S10, doi:10.1029/2007JA012774.
Trenchi, L., M. F. Marcucci, and R. C. Fear (2015), The effect of diamagnetic drift on motion of the dayside magnetopause reconnection line, *Geophys. Res. Lett.*, *42*, 6129–6136, doi:10.1002/2015GL065213.
Tsyganenko, N. A., and D. P. Stern (1996), Modeling the global magnetic field of the large-scale Birkeland current systems, *J. Geophys. Res.*, *101*, 27,187–27,198, doi:10.1029/96JA02735.
Vasyliunas, V. M. (1975), Theoretical models of magnetic field line merging, *Rev. Geophys.*, *13*(1), 303–336, doi:10.1029/RG013i001p00303.
Vines, S. K., S. A. Fuselier, K. J. Trattner, S. M. Petrinec, and J. F. Drake (2015), Ion acceleration dependence on magnetic shear angle in dayside magnetopause reconnection, *J. Geophys. Res. Space Physics*, *120*, 7255–7269, doi:10.1002/2015JA021464.
Walsh, B. M., T. D. Phan, D. G. Sibeck, and V. M. Souza (2014), The plasmaspheric plume and magnetopause reconnection, *Geophys. Res. Lett.*, *41*, 223–228, doi:10.1002/2013GL058802.